

Cite this: *CrystEngComm*, 2014, 16, 4816

# Structural library of coordination polymers based on flexible linkers exploiting the role of linker coordination angle: synthesis, structural characterization and magnetic properties†

Bharat Kumar Tripuramallu, Paulami Manna and Samar K. Das\*

Herein we report six new coordination polymers [Co(1,2-pda)(1,2-bix)]<sub>n</sub> (**1a**), [Co(hfipbb)(1,2-bix)]<sub>n</sub>·*n*H<sub>2</sub>O (**2a**), [Co(ADA)(1,2-bix)]<sub>n</sub> (**3a**), [Co(ADA)(1,3-bix)]<sub>n</sub>·*n*H<sub>2</sub>O (**3b**), [Co(1,4-pda)<sub>2</sub>(2-ptzt)]<sub>2</sub>[Co(H<sub>2</sub>O)<sub>6</sub>]<sub>2</sub>·2*n*H<sub>2</sub>O (**4a**), [Co<sub>2</sub>(μ-OH)(1,3-pda)(4-ptz)]<sub>n</sub> (**4b**) based on the flexible carboxylate ligands 1,2-phenylenediacetic acid (1,2-H<sub>2</sub>pda), 1,3-phenylenediacetic acid (1,3-H<sub>2</sub>pda), 1,3-adamantanediacyclic acid (H<sub>2</sub>ADA), 4,4'-(hexafluoroisopropylidene)bis(benzoic acid) (H<sub>2</sub>hfipbb) and secondary N-donor ligands 1,3-bis(imidazole-1-ylmethyl)-benzene (1,3-bix), 1,2-bis(imidazole-1-ylmethyl)-benzene (1,2-bix), 5-(4-pyridyl) tetrazole (4-ptz) and 2-(2H-tetrazol-5-yl)pyrazine (2-ptzt). All the compounds were characterized by single crystal X-ray diffraction analysis, IR spectroscopy, elemental analysis and bulk homogeneity by powder X-ray diffraction. A subtle relation between the position of the coordinating groups in the linker (known as linker coordination angle, LCA) and the dimensionality and topology of the final architectures of the title compounds has been discussed systematically by comparing with the structurally related reported compounds [Co(1,4-pda)(1,4-bix)]<sub>n</sub> (**1b**), [Co(hfipbb)(1,4-bix)<sub>0.5</sub>]<sub>n</sub> (**2b**) and [Co<sub>2</sub>(μ-OH)(1,4-pda)(4-ptz)]<sub>n</sub>·*n*H<sub>2</sub>O (**4c**). The compounds studied in the present work are classified into four different mixed linker classes, based on the skeleton geometry of the linker. Finally, temperature dependent magnetic susceptibility measurements have been studied and the relevant zero-field splitting parameters have been determined.

 Received 27th December 2013,  
Accepted 5th February 2014

DOI: 10.1039/c3ce42637h

[www.rsc.org/crystengcomm](http://www.rsc.org/crystengcomm)

## Introduction

Because of the enormous varieties of fascinating structural topologies and great potential applications as solid functional materials, metal organic frameworks (MOFs) and coordination polymers (CPs) have attracted considerable attention in recent years.<sup>1</sup> One of the most successful design strategies for constructing CPs is to take advantage of the versatility of several bridging ligands. Organic ligands with well-defined geometries may greatly influence the final structures of coordination polymers (CPs).<sup>2</sup> In the case of designing coordination polymers by using mixed linkers, the position of the coordinating groups on the linker often plays a major role in directing the dimensionality.<sup>3</sup> The general positions

of the coordinating groups in a simple phenyl linker are *ortho*-, *meta*-, and *para*-bidentate modes. The angle between the positions of the coordinating groups in the linker, which is known as the linker coordination angle (LCA), varies according to the geometry of the spacer; as a result, the overall coordination geometry of the concerned linker in the resulting CP alters, for example, bent, linear, *etc.* Zhou and co-workers reported the application of a mixture of bridging linkers with different LCAs in a coordination-driven self assembly process.<sup>4</sup> Coordination networks, based on rigid ligands exploiting LCAs, have been studied extensively due to their regular and well defined coordination modes.<sup>5</sup> In contrast, coordination polymers constructed using flexible ligands are still limited, because of the unpredictable nature of such systems arising from the flexible nature of spacers that allows more of degrees of freedom.<sup>6</sup>

Currently considerable efforts have been devoted to enriching the structural library of coordination networks based on flexible ligands. The major parameters to be considered in designing ditopic flexible ligand based coordination networks are the nature of the secondary ligand, coordination availability at the metal coordination sphere, length of the spacer and position of the coordinating groups. All these

School of Chemistry, University of Hyderabad, P.O. Central University, Hyderabad- 500046, India. E-mail: skdsc@uohyd.ernet.in, samar439@gmail.com; Fax: +91 40 2301 2460; Tel: +91 40 2301 1007

† Electronic supplementary information (ESI) available: Complete list of bond lengths and bond angles, 1/χ<sub>M</sub> vs. *T* plots, powder X-ray diffraction patterns, TGA curves and diffuse reflectance spectra and X-ray crystallographic data for compounds **1a**, **2a**, **3a**, **3b**, **4a** and **4b**; CCDC 978685–978690. For ESI and crystallographic data in CIF or other electronic format see DOI: 10.1039/c3ce42637h

factors have a tendency to modulate the conformations of the flexible ligands which is primarily responsible for the formation of higher dimensional structures. In ditopic flexible linkers, the geometrical orientation of two coordinating groups, associated with the secondary linker, results in the construction of coordination networks of varying topologies that can exhibit unique functional properties. Cao and co-workers reported a series of coordination polymers based on flexible ligands and used these compounds as functional materials for potential applications.<sup>7</sup> In our previous reports, we have discussed the factors affecting the conformational modulation of flexible ligands by exploring the role of the secondary linker and metal ion.<sup>8</sup> Cao's group and we have demonstrated conformational control of a flexible ligand, H<sub>2</sub>pda (*trans* to *cis* conformation) by introducing a rigid auxiliary ligand, e.g., 4,4'-bipyridine/rigid tetrazole linker.<sup>8,9</sup> Shi and coworkers reported a series of Zn(II) coordination polymer containing compounds from isomeric phenylenediacetic acid (1,4-, 1,3-, 1,2-H<sub>2</sub>pda) and dipyriddy ligands.<sup>10</sup> The literature reports of mixed linker coordination networks, based on flexible linkers exploiting the position of the coordinating groups in the linker, are very rare. We have been primarily working on coordination networks based on flexible linkers and reported our thoughts (in a conceptual manner) during analyzing the self-assembly processes of flexible linkers and transition metal ions that we have used in our laboratory.<sup>11</sup>

This concept prompted us to study the influence of the linker coordination angles (LCAs) of various flexible ligands in designing coordination networks of versatile topologies. We have chosen diverse linkers, e.g., flexible phenylene diacetates,<sup>12</sup> bent flexible adamantane diacetic acid,<sup>13</sup> bent 4,4'-(hexa-fluoroisopropylidene)bis(benzoic acid),<sup>14</sup> flexible bisimidazolyl nitrogen donors,<sup>15</sup> and rigid tetrazoles<sup>16</sup> in exploring the library of coordination networks with possible varied linker coordination angles. We have described the design and synthesis of a new series of coordination polymer containing compounds: [Co(1,2-pda)(1,2-bix)]<sub>n</sub> (**1a**), [Co(hfipbb)(1,2-bix)]<sub>n</sub>·nH<sub>2</sub>O (**2a**), [Co(ADA)(1,2-bix)]<sub>n</sub> (**3a**), [Co(ADA)(1,3-bix)]<sub>n</sub>·nH<sub>2</sub>O (**3b**), [Co(2-pztz)(1,4-pda)]<sub>2</sub>[Co(H<sub>2</sub>O)<sub>6</sub>]·2nH<sub>2</sub>O (**4a**) and [Co<sub>2</sub>(μ-OH)(1,3-pda)(4-ptz)]<sub>n</sub> (**4b**). In order to understand the affect of linker coordination angle (LCA), the above-mentioned compounds (present work) are compared with three other compounds reported earlier by us,<sup>8</sup> namely [Co(1,4-pda)(1,4-bix)]<sub>n</sub> (**1b**) [Co(hfipbb)(1,4-bix)]<sub>0.5</sub><sub>n</sub> (**2b**) and [Co<sub>2</sub>(μ-OH)(1,4-pda)(4-ptz)]<sub>n</sub>·nH<sub>2</sub>O (**4c**). In the present study, the mixed coordination networks are broadly classified into four different classes based on the geometry of their skeleton, as (flexible, flexible), (bent, flexible), (bent flexible, flexible) and (rigid, flexible); the first term in the bracket corresponds to the carboxylate linker and the second term to the secondary N-donor linker. Additionally, the magnetic exchange interactions between the metal centers and single ion anisotropy of the compounds are characterized through variable temperature magnetic susceptibility measurements and the relevant results have been described.

## Experimental section

### Materials and methods

All the chemicals were received as reagent grade and used without any further purification. The ligands 1,4-bix, 1,3-bix, 1,2-bix, 4-ptz, 2-tzpz were prepared according to the literature procedures.<sup>17</sup> Elemental analyses were determined by a FLASH EA series 1112 CHNS analyzer. Infrared spectra of solid samples were obtained as KBr pellets on a JASCO – 5300 FTIR spectrophotometer. Powder X-ray diffraction patterns were recorded on a Bruker D8-Advance diffractometer using graphite monochromated CuK<sub>α1</sub> (1.5406 Å) and K<sub>α2</sub> (1.54439 Å) radiation. Magnetic susceptibilities were measured in the temperature range 2–300 K on a Quantum Design VSM-SQUID. All compounds were synthesized in 23 mL Teflon-lined stainless vessels (Thermocon, India).

### Synthesis of [Co(1,2-pda)(1,2-bix)]<sub>n</sub> (**1a**)

A mixture of CoCl<sub>2</sub>·6H<sub>2</sub>O (0.25 mmol, 59.5 mg), 1,2-pda (0.25 mmol, 48.5 mg) and 1,2-bix (0.25 mmol, 60.0 mg) was dissolved in 10.0 mL of distilled water and the pH of the reaction mixture was adjusted to 6.35 by 0.5 M NaOH solution. Then the resulting mixture was stirred for 30 min and transferred to a 23 mL Teflon-lined stainless vessel, sealed, and heated at 160 °C for 72 h and then cooled to room temperature over 48 h to obtain red block crystals. Yield: 60.3% (based on Co). Anal. calcd for C<sub>24</sub>H<sub>22</sub>CoN<sub>4</sub>O<sub>4</sub> (M<sub>r</sub> = 489.39): C, 58.90%; H, 4.53%; N, 11.44%. Found: C, 58.45%; H, 4.35%; N, 11.01%. IR (KBr pellet, cm<sup>-1</sup>): 3140, 2997, 2916, 1695, 1572, 1520, 1369, 1265, 1226, 1024, 949, 852, 810, 748, 721, 657.

### Synthesis of [Co(hfipbb)(1,2-bix)]<sub>n</sub>·nH<sub>2</sub>O (**2a**)

A mixture of CoCl<sub>2</sub>·6H<sub>2</sub>O (0.25 mmol, 59.5 mg), H<sub>2</sub>hfipbb (0.25 mmol, 98.0 mg) and 1,2-bix (0.25 mmol, 60.0 mg) was dissolved in a solvent mixture of H<sub>2</sub>O (10.0 mL) + DMF (1.0 mL) and stirred for 30 min. The pH of the reaction mixture was adjusted to 6.10 by adding 5 M NaOH solution and the resulting reaction mixture was placed in a 23 mL Teflon-lined stainless steel autoclave, which was sealed and heated at 160 °C for 72 h. The autoclave was allowed to cool to room temperature for 48 h. Deep blue colored block-shaped crystals of compound **2a** were obtained in a 65.5% yield (based on Co). Anal. calcd for C<sub>31</sub>H<sub>22</sub>N<sub>4</sub>F<sub>6</sub>O<sub>5</sub>Co (M<sub>r</sub> = 703.46): C, 52.93%; H, 3.15%; N, 7.96%. Found: C, 52.65%; H, 2.98%; N, 7.48%. IR (KBr pellet, cm<sup>-1</sup>): 3516, 3138, 3015, 1699, 1612, 1556, 1518, 1462, 1244, 1170, 1091, 968, 949, 777, 717, 653.

### Synthesis of {Co(ADA)(1,2-bix)}<sub>n</sub> (**3a**)

A mixture of CoCl<sub>2</sub>·6H<sub>2</sub>O (0.25 mmol, 59.5 mg), H<sub>2</sub>ADA (0.25 mmol, 63.3 mg) and 1,2-bix (0.25 mmol, 60.0 mg) in H<sub>2</sub>O:MeOH (10:1) was stirred for 30 min and sealed in a 25 mL Teflon-lined stainless steel autoclave (pH = 7.00). The resulting reaction mixture was heated at 130 °C for 4 days, and then slowly cooled to room temperature. Blue crystals of

**3a** were obtained in a 60.3% yield (based on Co). Anal. calcd for  $C_{28}H_{30}CoN_4O_4$  ( $M_r = 545.49$ ): C, 61.65%; H, 5.54%; N, 10.27%. Found: C, 61.49%; H, 5.35%; N, 10.42%. IR (KBr pellet,  $cm^{-1}$ ): 3408, 3128, 3101, 2962, 2904, 2838, 1672, 1572, 1528, 1446, 1402, 1254, 1101, 953, 750, 723, 673.

#### Synthesis of $\{Co(ada)(1,3-bix)\}_n$ (**3b**)

The ligand 1,2-bix was replaced by ligand 1,3-bix (0.25 mmol, 60.0 mg) and allowed to react with  $CoCl_2 \cdot 6H_2O$  (0.25 mmol, 59.5 mg) and  $H_2ADA$  (0.25 mmol, 63.3 mg) to obtain the compound **3b** and blue crystals were filtered off in a 40% yield (based on Co). Anal. calcd for  $C_{28}H_{34}CoN_4O_5$  ( $M_r = 565.52$ ): C, 59.47%; H, 6.060%; N, 9.907%. Found: C, 59.23%; H, 6.11%; N, 9.76%. IR (KBr pellet,  $cm^{-1}$ ): 3452, 3397, 3150, 3095, 2838, 1649, 1545, 1523, 1446, 1419, 1358, 1232, 1150, 1112, 942, 816, 739, 657.

#### Synthesis of $[Co(2-ptzt)(1,4-pda)_2]_2[Co(H_2O)_6] \cdot 2nH_2O$ (**4a**)

A mixture of  $CoCl_2 \cdot 6H_2O$  (0.50 mmol, 119.0 mg), 1,4-pda (0.25 mmol, 48.5 mg) and 2-ptzt (0.25 mmol, 37 mg), dissolved in  $H_2O$  (10.0 mL), was stirred for 30 min and the pH of the reaction mixture was adjusted to 5.4 by adding 5 M NaOH solution. The reaction mixture was placed in a 23 mL Teflon-lined stainless steel autoclave, sealed and heated at 130 °C for 96 h. The autoclave was allowed to cool to 30 °C for 48 h. Deep red block-shaped crystals of compound **4a** were obtained in a 65.5% yield (based on Co). Anal. calcd for  $C_{30}H_{38}Co_3N_{12}O_{16}$  ( $M_r = 999.51$ ): C, 36.05%; H, 3.83%; N, 16.81%. Found: C, 35.15%; H, 3.24%; N, 16.69%. IR (KBr pellet,  $cm^{-1}$ ): 3362, 3026, 2926, 1684, 1616, 1574, 1523, 1410, 1253, 1170, 972, 935, 842, 746.

#### Synthesis of $[Co_2(\mu-OH)(1,3-pda)(4-ptz)]_n$ (**4b**)

A mixture of  $CoCl_2 \cdot 6H_2O$  (0.50 mmol, 119 mg), 1,3-pda (0.25 mmol, 48.5 mg) and 4-ptz (0.25 mmol, 36.65 mg) was dissolved in 10 mL distilled  $H_2O$  which was adjusted to pH = 4.20 with 5 M NaOH solution. The resulting final reaction mixture was sealed in a 23 mL Teflon-lined stainless steel autoclave and heated at 130 °C for 3 days. Dark red block-shaped crystals were obtained, filtered off and collected in a 55.2% yield. Anal. calcd for  $C_{16}H_{12}Co_2N_5O_5$  ( $M_r = 472.17$ ): C, 40.70%; H, 2.56%; N, 14.83%. Found: C, 40.15%; H, 2.02%; N, 14.09%. IR (KBr pellet,  $cm^{-1}$ ): 3574, 1614, 1601, 1442, 1419, 1394, 1290, 1221, 974, 842, 760, 715, 630.

#### Single crystal X-ray structure determination of the compounds

Crystal data of the compounds **1a**, **3a**, **3b**, and **4b** were collected on an Oxford Xcalibur Gemini Eos CCD diffractometer at 298 K using Mo-K $\alpha$  radiation ( $\lambda = 0.7107 \text{ \AA}$ ). Data reduction was performed using CrysAlisPro (version 1.171.33.55)<sup>18a</sup> and SHELXL-97 was used to refine the structures. The compounds **2a** and **4a** were mounted on a three circle Bruker SMART-APEX CCD area detector system under a Mo-K $\alpha$  ( $\lambda = 0.71073 \text{ \AA}$ )

graphite monochromated X-ray beam with a crystal to detector distance of 60 mm, and a collimator of 0.5 mm. The scans were recorded with an  $\omega$  scan width of 0.3°. Data reduction was performed by SAINTPLUS.<sup>18b</sup> Intensities were corrected for absorption using SADABS.<sup>18c</sup> The structures were solved using SHELXS-97<sup>18d</sup> and full-matrix least-squares refinements were performed using SHELXL-97.<sup>18e</sup> All the non-hydrogen atoms were refined anisotropically. Hydrogen atoms on the C atoms were introduced in calculated positions and were included in the refinement riding on their respective parent atoms. Crystal data and structure refinement parameters for all the compounds are summarized in Table 1. A complete list of bond lengths and bond angles are given in the section of ESI.†

## Results and discussion

### Synthesis

In order to exploit the role of the linker coordination angles (LCAs) in the coordination polymers, based on flexible linkers, we chose the following linkers: phenylenediacetates, isomeric bis(imidazole-1-ylmethyl)-benzene linkers, bent flexible carboxylate linker 1,3-adamantane diacetic acid, bent carboxylate linker  $H_2hfipbb$  and rigid tetrazoles. The title compounds were synthesized under hydrothermal conditions and the reaction procedures were optimized to obtain the best yields.  $CoCl_2 \cdot 6H_2O$  was taken as the metal source in the synthesis of the compounds due to its versatility in forming octahedral, square pyramidal and tetrahedral coordination geometries. The syntheses of the compounds were performed at 160 °C for **1a** and **2a**, and 130 °C for **3a**, **3b**, **4a** and **4b** in an aqueous medium.

### Linker coordination angle (LCA)

In ditopic linkers, the coordination angle between the positions of two coordinating groups in a linker is called the linker coordination angle. For a simple rigid phenyl linker, three different linker coordination angles (*i.e.* 60°, 120°, and 180°) are possible between the two coordinating groups. Different terminologies are used to represent the position of the coordinating groups in the linker such as, *ortho*, *meta*, *para* and (1,4)-, (1,3)-, and (1,2)- *etc.* In the case of designing coordination architectures with mixed linkers, the LCAs of both the linkers should be considered in obtaining the desired topologies. The task becomes more difficult in the case of flexible ditopic linkers, as they have more degrees of freedom.

To reduce the complexity in measuring the linker coordination angle for flexible linkers, we have considered the angle between the two atoms of the linker where the coordinating groups are connected, for example, the LCA of 1,3-pda is measured as the angle between two  $CH_2$  groups of the acetate side chains with respect to the benzene ring, which is 120°. An important point to remember in quantifying the LCA is that it is different from the dihedral angle between the two coordinating groups and the angle between two coordinating atoms. The LCAs of the ligands phenylenediacetates, bis(imidazole-1-ylmethyl)-benzene, bent

**Table 1** Crystal data and structural refinement parameters for compounds

	1a	2a	3a
Empirical formula	C <sub>24</sub> H <sub>22</sub> CoN <sub>4</sub> O <sub>4</sub>	C <sub>31</sub> H <sub>22</sub> N <sub>4</sub> F <sub>6</sub> O <sub>5</sub> Co	C <sub>28</sub> H <sub>30</sub> CoN <sub>4</sub> O <sub>4</sub>
Formula weight	489.39	703.46	545.49
<i>T</i> (K)/ $\lambda$ (Å)	298(2), 0.71073	298(2), 0.71073	298(2), 0.71073
Crystal system	Monoclinic	Orthorhombic	Monoclinic
Space group	<i>P</i> 2 <sub>1</sub> / <i>c</i>	<i>Ccca</i>	<i>P</i> 2(1)/ <i>c</i>
<i>a</i> (Å)	8.5118(7)	13.177(8)	11.5867(3)
<i>b</i> (Å)	22.703(2)	15.668(8)	12.6968(4)
<i>c</i> (Å)	11.3906(8)	18.950 (16)	17.5141(5)
$\alpha$ (°)	90.00	90.00	90.00
$\beta$ (°)	105.401(7)	90.00	96.216(3)
$\gamma$ (°)	90.00	90.00	90.00
Volume (Å <sup>3</sup> )	2122.1(3)	5977(5)	2561.42(13)
<i>Z</i> , $\rho_{\text{calcd}}$ (g cm <sup>-3</sup> )	4, 1.532	8, 1.563	4, 1.415
$\mu$ (mm <sup>-1</sup> ), <i>F</i> (000)	0.850/1012	0.660/2856	0.712/1140
Goodness-of-fit on <i>F</i> <sup>2</sup>	1.034	1.248	1.056
<i>R</i> <sub>1</sub> / <i>wR</i> <sub>2</sub> [ <i>I</i> > 2 $\sigma$ ( <i>I</i> )]	0.0535/0.0934	0.0687/0.1377	0.0398/0.1043
<i>R</i> <sub>1</sub> / <i>wR</i> <sub>2</sub> (all data)	0.0875/0.1061	0.0867/0.1440	0.0529/0.1123
Largest diff peak/hole (e Å <sup>-3</sup> )	0.401/−0.313	0.618/−0.307	0.627/−0.227
	<b>3b</b>	<b>4a</b>	<b>4b</b>
Empirical formula	C <sub>28</sub> H <sub>34</sub> CoN <sub>4</sub> O <sub>5</sub>	C <sub>30</sub> H <sub>38</sub> Co <sub>3</sub> N <sub>12</sub> O <sub>16</sub>	C <sub>16</sub> H <sub>13</sub> N <sub>5</sub> O <sub>5</sub> Co <sub>2</sub>
Formula weight	565.52	999.51	473.17
<i>T</i> (K)/ $\lambda$ (Å)	298(2), 0.71073	298(2), 0.71073	298(2), 0.71073
Crystal system	Monoclinic	Triclinic	Monoclinic
Space group	<i>P</i> 2(1)/ <i>n</i>	<i>P</i> $\bar{1}$	<i>P</i> 2 <sub>1</sub> / <i>n</i>
<i>a</i> (Å)	13.1976(9)	9.3717(8)	8.9732(4)
<i>b</i> (Å)	10.4914(7)	10.1843(9)	20.4712(9)
<i>c</i> (Å)	20.3760(15)	11.7377(11)	10.4084(5)
$\alpha$ (°)	90.00	112.9560(10)	90.00
$\beta$ (°)	108.808(8)	106.240(2)	102.998(5)
$\gamma$ (°)	90.00	90.6960(10)	90.00
Volume (Å <sup>3</sup> )	2670.6(3)	967.32(15)	1862.95(15)
<i>Z</i> , $\rho_{\text{calcd}}$ (g cm <sup>-3</sup> )	4, 1.407	1, 1.716	4, 1.687
$\mu$ (mm <sup>-1</sup> ), <i>F</i> (000)	0.688, 1188	1.360, 511	1.819, 948
Goodness-of-fit on <i>F</i> <sup>2</sup>	1.024	1.027	1.109
<i>R</i> <sub>1</sub> / <i>wR</i> <sub>2</sub> [ <i>I</i> > 2 $\sigma$ ( <i>I</i> )]	0.0440/0.1027	0.0322/0.0767	0.0448/0.1063
<i>R</i> <sub>1</sub> / <i>wR</i> <sub>2</sub> (all data)	0.0653/0.1166	0.0385/0.0802	0.0565/0.1120
Largest diff peak/hole (e Å <sup>-3</sup> )	0.422/−0.376	0.357/−0.229	0.879/−0.302

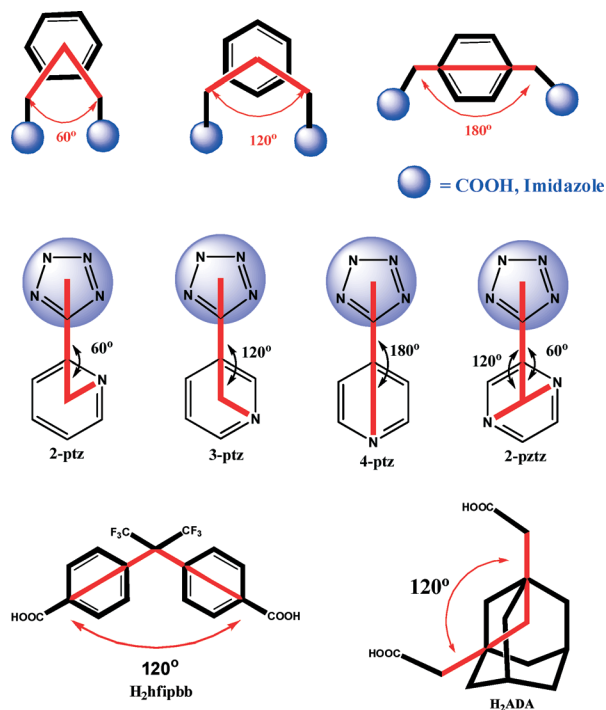
carboxylate ligands H<sub>2</sub>hfipbb and H<sub>2</sub>ADA and rigid tetrazoles employed in this work are shown in the following Scheme 1 and Table 2

In the case of tetrazole ligands, as shown in Scheme 1, the LCA is measured between the tetrazole core ring and the position of the nitrogen atom in the pyridine ring. The LCAs mentioned in the above linkers are considered in their ideal geometry but in actual case, these angles will vary to  $\pm 10^\circ$  based on the coordination consequences adopted by the linkers, *e.g.*, hfipbb<sup>2-</sup> will have LCAs of 111°, 108° *etc.*, ADA<sup>2-</sup> has LCAs of 118°, 122° *etc.* In our previous article, we reported the factors affecting the conformational modulation of flexible linkers in the self-assembly of coordination networks,<sup>8</sup> in which only a few flexible linkers were used to explain these factors, but in order to rationalize this concept of flexibility in terms of coordination and dimensionality, an elaborated study is required. In view of this, in this article, we have demonstrated a library of coordination networks exploring the possible flexible linkers with rigid and bent secondary ligands.

## Description of crystal structures

### (Flexible, flexible)

[Co(1,2-pda)(1,2-bix)]<sub>*n*</sub> (1a) and [Co(1,4-pda)(1,4-bix)]<sub>*n*</sub> (1b). Compound 1b is a 3D coordination polymer and the structural details have been previously reported,<sup>8</sup> whereas, compound 1a is a 2D coordination polymer containing compound, that crystallizes in the monoclinic space group *P*2<sub>1</sub>/*c*. The asymmetric unit consists of one crystallographically independent Co(II) atom in a distorted tetrahedral geometry, one 1,2-pda<sup>2-</sup> ligand and one 1,2-bix ligand. The distortion parameter  $\tau_4$  (= 0.87), calculated by the four-coordinate geometry index ( $\tau_4 = \{360^\circ - (\alpha + \beta)\}/141$ , where  $\alpha$  and  $\beta$  are the two largest angles of the tetrahedra), indicates slight distortion in its tetrahedral geometry.<sup>18f</sup> The tetrahedral geometry around the Co(II) atom is comprised of two oxygen atoms from two different 1,2-pda<sup>2-</sup> ligands and two nitrogen atoms from two different 1,2-bix ligands (Fig. 1a). The carboxylate linker 1,2-pda<sup>2-</sup> coordinates to the Co(II) center in  $\mu_1$ - $\eta_1, \eta_0$  coordination mode on either side and connects the adjacent Co(II) tetrahedra in a typical *trans* conformation with an anticlinal torsion angle of



**Scheme 1** Schematic representation of linker coordination angles of the flexible linkers employed in this study.

132.64° (viewed through N4–C24–C14–N2). The acetate side chains twist with respect to the phenyl ring through various extents *i.e.* 101.46° (through C4–C3–C2–C1) and 96.92° (through C7–C8–C9–C10). 1,2-pda<sup>2-</sup> separates the two Co(II) centers with a distance of 8.512 Å to form a 1D metal–acid chain along the crystallographic *a* axis (Fig. 1b). These adjacent chains are connected to each other with the aid of 1,2-bix ligands along the *b* axis to form a 2D layer in the *ab* plane. 1,2-Bix connects the Co(II) atoms of the adjacent chains in a typical *trans* conformation with an antiperiplanar torsion angle of 151.22° (viewed through N4–C24–C14–N2) and creates separation of 12.114 Å between the two metal centers in the adjacent chains. The dihedral angles between the imidazole ring planes and the least-squares plane of the phenyl group are 74.01° and 77.50°, respectively. The connectivity of the 1,2-bix to the metal acid chains results in the formation of 2D (4,4) connected sheets with dimensions of 12.114 × 8.512 Å<sup>2</sup> (Fig. 1c). The linker coordination angle between the two imidazole rings in 1,2-bix is 60°, and due to the shorter distance between the two coordinating N atoms it has a tendency to

adopt a *cis* conformation to form a molecular box, but in this case, 1,2-bix adopts a *trans* conformation, thereby forming 2D layers. The presence of flexibility in the ligands employed, results in the formation of a wave like layer with crests and troughs at the metal acid chains. These layers are stacked along the *c* axis in an ABAB fashion and the adjacent layers are tilted to ~7 Å and the alternate layers are arranged in a back-to-back fashion as shown in Fig. 1d.

### (Bent, flexible)

[Co(hfipbb)(1,2-bix)]<sub>n</sub>·*n*H<sub>2</sub>O (2a) and [Co(hfipbb)(1,4-bix)<sub>0.5</sub>]<sub>n</sub> (2b). Compound 2a is a 2D extended coordination polymer crystallizing in the orthorhombic space group *ccca*. Compound 2b is a 3D layered pillared framework, as described in our previous report,<sup>8</sup> in which the 2D metal–hfipbb layers are pillared by the 1,4-bix linkers. The structural details and crystallographic details of 2b have been reported; herein we have discussed only compound 2a. The molecular diagram of 2b consists of the Co(II) atom in a slightly distorted tetrahedral {CoN<sub>2</sub>O<sub>4</sub>} geometry with a  $\tau_4$  of 0.93, constituted by the oxygen atoms from two different hfipbb<sup>2-</sup> units,<sup>19</sup> and nitrogen atoms from two different 1,2-bix<sup>20</sup> ligands and one lattice water molecule as shown in the Fig. 2a. The bond distances of Co–O and Co–N are in the range 1.957(3)–2.023(3) Å and the bond angles around the Co(II) centre are in the range 100.17°–112.32°. The carboxylate groups in H<sub>2</sub>hfipbb are completely deprotonated and each carboxylate group in hfipbb<sup>2-</sup> coordinates to the metal center in  $\mu_1$ - $\eta_1$ , $\eta_0$  coordination mode by creating a separation of 13.17 Å between the two metal centers. The dihedral angle between the two benzene rings in the hfipbb<sup>2-</sup> anion is 74.77°, which is higher than that of 68.57° in the neutral H<sub>2</sub>hfipbb ligand. The connectivity of hfipbb<sup>2-</sup> with the metal centers results in the formation of 1D metal acid zig-zag chains along the crystallographic *b* axis as shown in Fig. 2b. The metal–hfipbb systems are very well known in the literature for the formation of paddle-wheel structures having open coordination sites at the metal apical position, which is used to extend the dimensionality by the N-donor ligands.<sup>14</sup> On the other hand, in the crystal structure of compound 1, metal–hfipbb forms 1D chains, that are extended to form 2D (4,4) connected sheets with the aid of 1,2-bix ligands.<sup>15</sup> The 1,2-bix ligand connects the Co(II) atoms of the adjacent 1D chains in a typical *trans* conformation with an antiperiplanar torsion angle of 151.84° (viewed through N2–C13–C13–N2) and creates a separation of 10.236 Å between the

**Table 2** Linker coordination angles of various linkers employed in this work (see Scheme 1)

Linker name	1,4-	1,3-	1,2-
<b>Flexible</b>			
pda	1,4-pda = 180° (linear)	1,3-pda = 120° (bent)	1,2-pda = 60° (chelated)
bix	1,4-bix = 180° (linear)	1,3-bix = 120° (bent)	1,2-bix = 60° (chelated)
H <sub>2</sub> ADA	120° (bent flexible)		
<b>Rigid</b>			
ptz	4-ptz = 180° (linear)	3-ptz = 120° (bent)	2-ptz = 60° (chelated)
H <sub>2</sub> hfipbb	120° (bent)		2-pztz = 60°, 120° (chelated, bent)

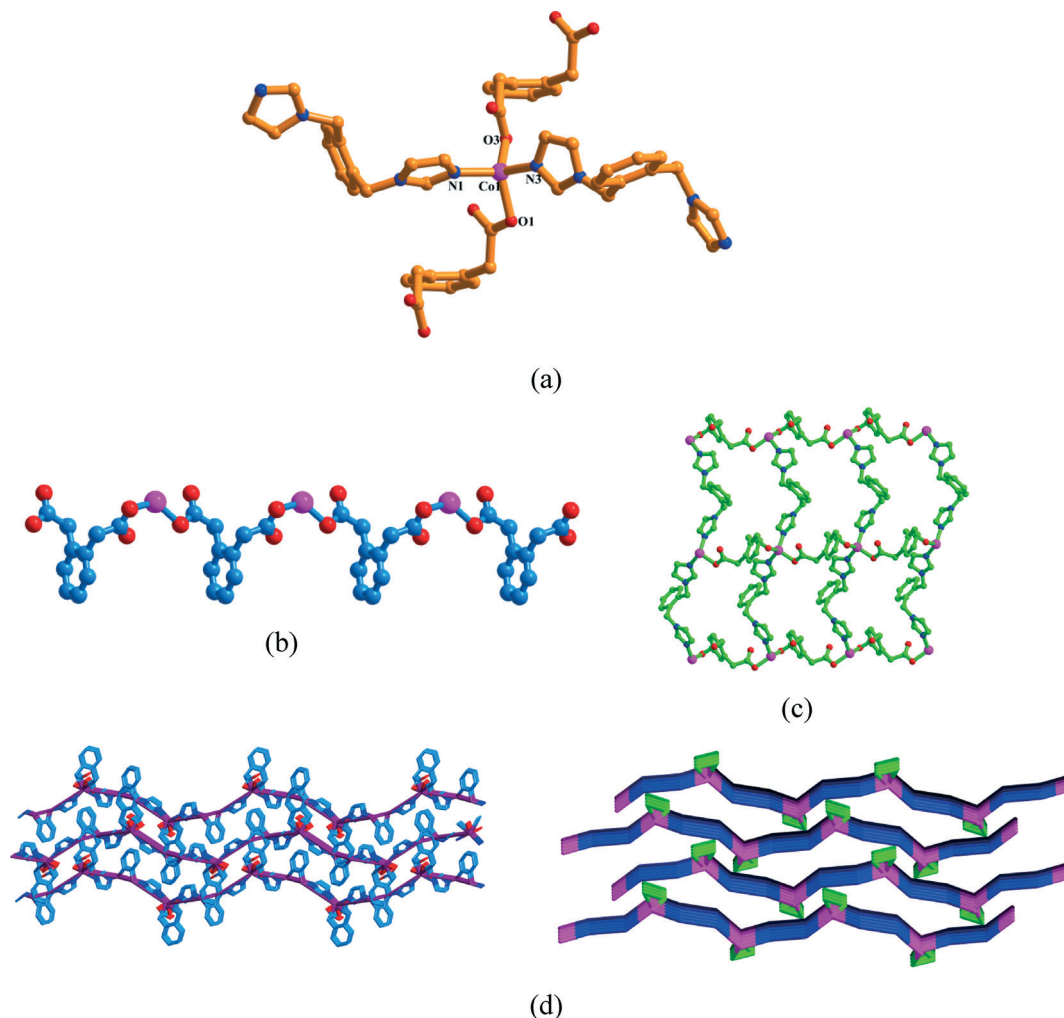


**Fig. 1** (a) Coordination environment around the  $\text{Co}^{\text{II}}$  ion in **1a** with hydrogen atoms omitted for clarity. (b) 1D zig-zag chains formed due to Co-1,2-pda connectivity. (c) The overall 2D (4,4) connected sheets. (d) 3D stacking of 2D layers showing the tilting between two layers and its topological representation.

two adjacent chains. The overall connectivity of the 1,2-bix ligands with the metal acid chains results in the formation of (4,4) corrugated sheets with dimensions of  $13.177 \times 10.236 \text{ \AA}^2$  (Fig. 2c). The  $\text{CF}_3$  groups, present on the  $\text{hfipbb}^{2-}$ , decorate the surface of the 2D layers. The corrugated nature of the 2D layers allows the two layers to stack over each other to form a double layer with  $\text{CF}_3$  groups above and below the double layer (Fig. 2d). These double layers are again stacked over each other resulting in the formation of two different types of cavities *i.e.*, fluorinated cavities, that are formed due to stacking of the double layers and non fluorinated cavities, formed due to the stacking of the monolayers as shown in Fig. 2e. Two solvent molecules per cavity are present in the crystal structure and located exactly on the plane of the monolayer; as a result they are present in the nonfluorinated cavity as shown in Fig. 2e.

#### (Bent flexible, flexible)

$\{\text{Co}(\text{ADA})(1,2\text{-bix})\}_n$  (**3a**). The bent flexible linker  $\text{H}_2\text{ADA}$  reacts with the  $\text{Co}(\text{II})$ -1,2-bix system, resulting in compound

**3a**. Although compound **3a** forms a 2D grid-like layer structure, in this compound,  $\text{Co}(\text{II})$  has a slightly distorted tetrahedral geometry instead of octahedral geometry with a distortion parameter  $\tau_4$  of 0.78. Each  $\text{Co}(\text{II})$  ion coordinates with two oxygen atoms from two different  $\text{ADA}^{2-}$  ligands and two N atoms from two 1,2-bix ligands (Fig. 3a). The bond distances of Co–O and Co–N are in the range 1.964(2)–2.057(6)  $\text{\AA}$  and the bond angles around the  $\text{Co}(\text{II})$  centre are in the range  $95.75^\circ$ – $106.30^\circ$ . Both carboxylate groups of the  $\text{ADA}^{2-}$  ligand adopt the  $\mu_1\text{-}\eta^1\text{:}\eta^0$  coordination mode and each carboxylate group connects one  $\text{Co}(\text{II})$  atom in a mono-dentate fashion. The adjacent  $\text{Co}(\text{II})$  atoms are connected by the  $\text{ADA}^{2-}$  ligand in *cis* conformation with a torsion angle of  $10.55^\circ$  (viewed through C1–C2–C14–C13) creating a  $\text{Co}\cdots\text{Co}$  separation of 6.925  $\text{\AA}$  affording a 1D chain through the *b* axis. Interestingly, these chains have alternating right and left turns along the pitch of the  $\text{ADA}^{2-}$  resulting in the formation of a 1D zig-zag structure (Fig. 3b). The  $\text{Co}(\text{II})$  centres in these chains are again connected by 1,2-bix along the *c* axis creating a separation of 13.648  $\text{\AA}$ . The 1,2-bix linker connects the  $\text{Co}(\text{II})$  centers

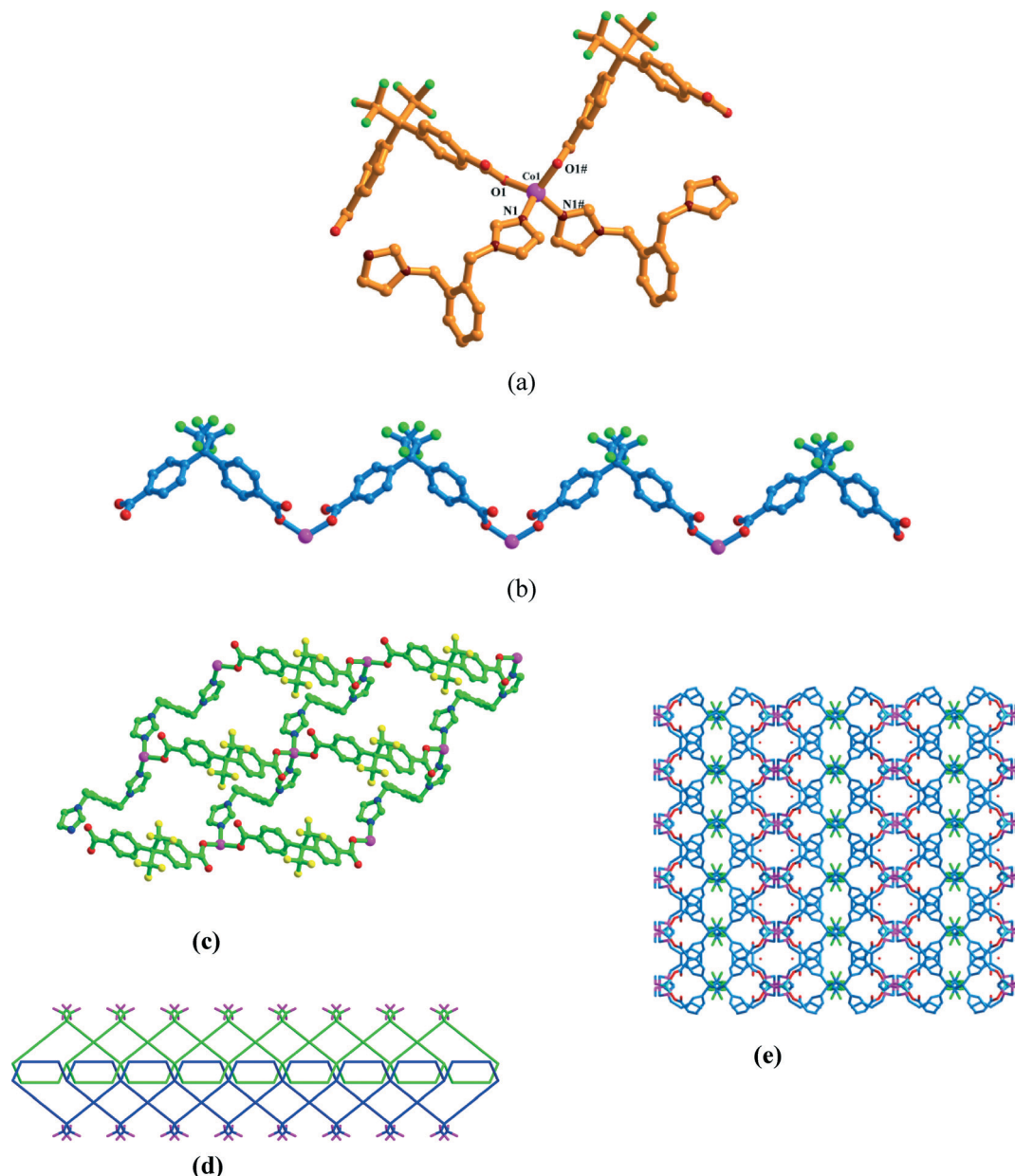


**Fig. 2** (a) Molecular diagram of compound **2a** with atom labeling at the coordination sphere and (b) 1D zig-zag chains formed due to Co-hfipbb connectivity. (c) 2D (4,4) connected topology viewing the square grid. (d) Stacking of two monolayers to form a double layer. (e) 3D stacking of double layers showing the two different types of cavities.

in a typical *cis* conformation in which the dihedral angle between the two imidazole rings is  $30.39^\circ$  and the dihedral angles between the imidazole rings and benzene rings are  $75.31^\circ$  and  $75.21^\circ$ , respectively. This associated connection of  $\text{ADA}^{2-}$  and 1,2-bix with the  $\text{Co(II)}$  centre results in a 2D grid like layer structure along the crystallographic *bc* plane. Due to the 1D zig-zag pattern of the  $\text{Co(II)}\text{-ADA}^{2-}$  chains, the parallelograms formed by the connectivity of 1,2-bix ligands result in two different dimensions (to be named A and B) as shown in Fig. 3c. Parallelogram A has a larger area with dimensions of  $18.265 \times 11.612 \text{ \AA}^2$  and B has a smaller area with dimensions of  $20.016 \times 8.234 \text{ \AA}$ . These parallelograms are arranged in an alternate ABAB fashion in both the

directions along the  $\text{Co(II)}\text{-ADA}^{2-}$  zig-zag chains and  $\text{Co(II)}\text{-1,2-bix}$  chains. These 2D layers perfectly stack on each other in an eclipsed manner to arrange the parallelograms to form 1D channels (Fig. 3d). In addition, intermolecular hydrogen bonding was observed between the C-H groups of the  $\text{ADA}^{2-}$  linkers of one layer and carboxylate O atoms of the  $\text{ADA}^{2-}$  linkers of another layer through  $\text{C8-H8}\cdots\text{O1}$  (with symmetry code  $2 - x, 0.5 + y, 0.5 - z$ ) with a bond distance of  $3.622 \text{ \AA}$ , along with some weak  $\text{C-H}\cdots\text{N}$  interactions between the C-H groups of the  $\text{ADA}^{2-}$  ligands and N atoms of the imidazole rings. Hence, the two dimensional layers are connected to each other through  $\text{C-H}\cdots\text{O}$  and  $\text{C-H}\cdots\text{N}$  interactions to form a 3D supramolecular framework.

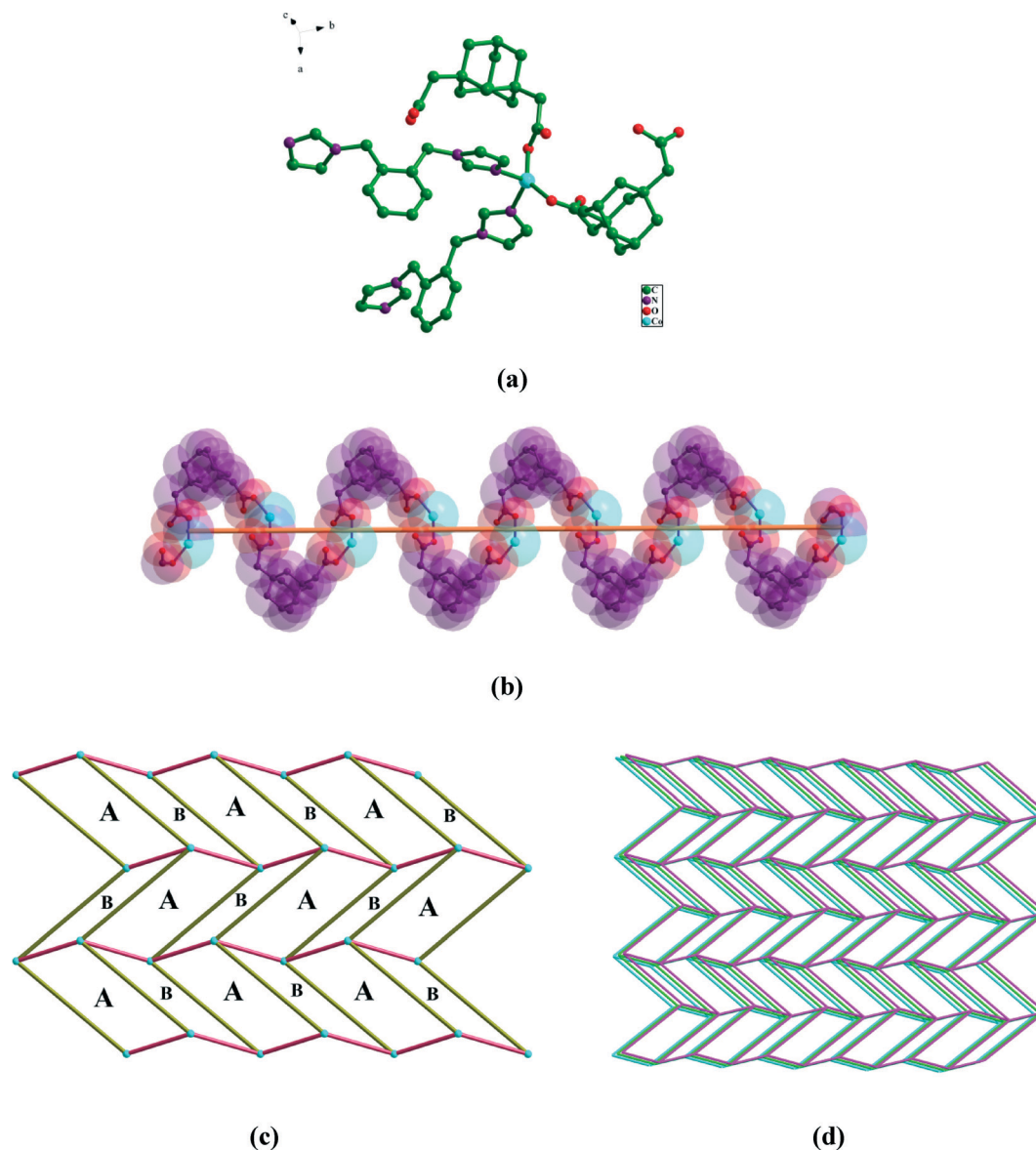
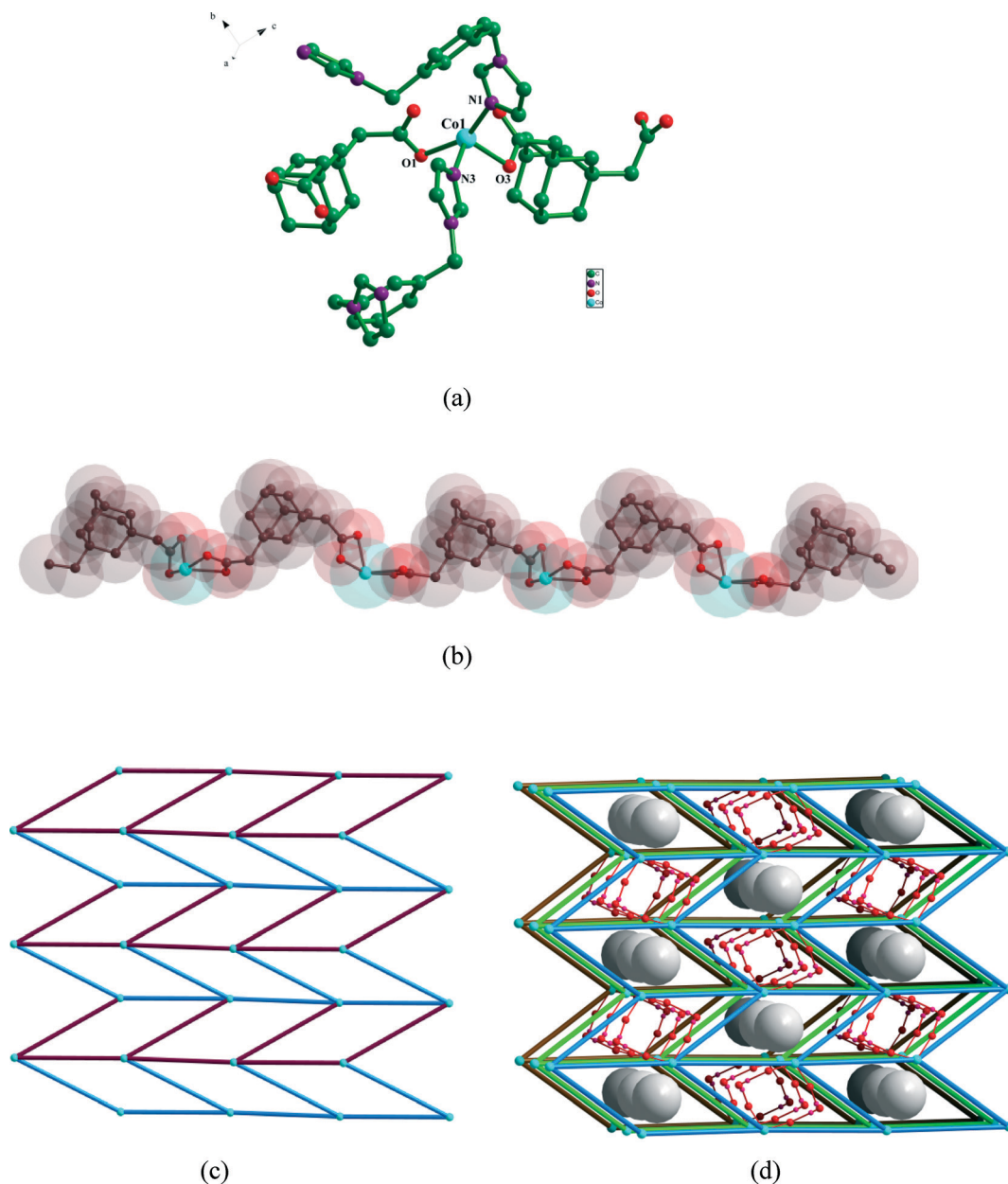


Fig. 3 (a) The immediate coordination environment of the Co(II) metal center in compound 3a. (b) 1D zig-zag chains formed due to Co-ADA connectivity. (c) 2D (4,4) connected topology viewing the square grid with two different types of the parallelograms. (d) 3D eclipsed stacking of layers.

$\{\text{Co}(\text{ADA})(1,3\text{-bix})\}_n \cdot n\text{H}_2\text{O}$  (3b). Compound 3b is obtained by replacing the ligand 1,2-bix (LCA  $60.0^\circ$ ) with 1,3-bix (LCA  $120.0^\circ$ ). The molecular diagram consists of the Co(II) ion in a distorted tetrahedral geometry with two O atoms from two different  $\text{ADA}^{2-}$  ligands, two N atoms from two different 1,3-bix ligands and a lattice water molecule (Fig. 4a). The distortion in the tetrahedral geometry around the Co(II) centre,  $\tau_4$ , is 0.73 which is considerably larger compared to the  $\tau_4$  values determined for compounds 1a, 2a and 3a. The Co(II)-O bond lengths are in the range 2.052–2.158 Å, and Co(II)-N bond lengths are in the range 2.062–2.082 Å, which are in good accordance with the literature. The bond angles around the Co(II) centre are in the range  $91.01\text{--}153.1^\circ$  indicating severe distortion in the tetrahedral geometry around the metal centre. In this compound, both carboxylate groups of the acetate side chains in  $\text{ADA}^{2-}$  adopt the  $\mu_1\text{-}\eta^1\text{:}\eta^0$

coordination mode and coordinate to the Co(II) centers by creating a separation of 10.19 Å. The acetate side chains in the  $\text{ADA}^{2-}$  linker adopt a *trans* conformation with a torsion angle of  $122.02^\circ$  (viewed through C15–C16–C27–C28). The connectivity of  $\text{ADA}^{2-}$  with the Co(II) centers results in the formation of 1D chains. In these Co(II)- $\text{ADA}^{2-}$  chains, all the adamantane rings are located on the same side of the axis unlike the zig-zag pattern observed in 3a (Fig. 4b). These 1D chains are connected by the 1,3-bix linker by coordination of the imidazole nitrogen atoms to the Co(II) centers to form 2D sheets. The ligand 1,3-bix is a 1,3-positioned ligand with an LCA of  $120.0^\circ$ , which exists in a *trans* conformation with a torsion angle of  $117.38^\circ$  and creates a separation of 11.14 Å between the two Co(II) centers of two adjacent Co(II)- $\text{ADA}^{2-}$  chains. The overall connectivity of the Co(II) centers with the  $\text{ADA}^{2-}$  and 1,3-bix ligands results in the formation of 2D (4,4)



**Fig. 4** (a) Molecular diagram of compound **3b** describing the coordination sphere. (b) 1D zig-zag chains formed due to Co–ADA connectivity. (c) 2D (4,4) connected topology viewing the square grid. (d) Figure viewing the eclipsed stacking of monolayers containing  $R_4^2(10)$  hydrogen bonding rings with the lattice water molecules in the channels and the empty channels.

connected corrugated sheets rather than planar sheets (Fig. 4c). The flexibility, present in the ligand 1,3-bix, imparts diagonal connectivity between the two Co(II) centres of adjacent chains instead of linear connectivity; as a result, the 1D Co(II)–ADA<sup>2-</sup> chains are arranged in a wavy ABAB fashion rather than a planar AAAA fashion. One lattice water molecule per molecular formula unit is present in the crystal structure. These lattice water molecules are present exactly on the plane of the sheets and located in the void spaces created by the (4,4) connectivity of the metal centers. Interestingly, two lattice water molecules per parallelogram are arranged in alternate parallelograms as shown in Fig. 4d. These lattice water

molecules form strong hydrogen bonding interactions between the carboxylate oxygens of the same sheets forming ten membered  $R_4^2(10)$  rings inside the parallelograms alternatively. However no hydrogen bonding is observed between the adjacent sheets through lattice water molecules.

#### (Flexible, rigid)

$[\text{Co}(1,4\text{-pda})_2(2\text{-pztz})]_2[\text{Co}(\text{H}_2\text{O})_6] \cdot 2n\text{H}_2\text{O}$  (**4a**). Compound **4a** is a 1D ion pair compound that crystallizes in the triclinic space group  $P\bar{1}$ . The molecular diagram consists of a 1D anionic chain  $[\text{Co}(2\text{-pztz})(1,4\text{-pda})_2]^{2-}$  and lattice cationic  $[\text{Co}(\text{H}_2\text{O})_6]^{2+}$

units. The repeating unit in the 1D chain consists of two crystallographically independent Co(II) atoms in *tbp* geometry bridged by two 2-pztz<sup>1-</sup> ligands<sup>21</sup> and connected to four 1,4-pda<sup>2-</sup> ligands (Fig. 5a). The *tbp* geometry of each Co(II) ion in the anionic chain is furnished by three nitrogen atoms from two different 2-pztz<sup>1-</sup> ligands in the basal plane and two 1,4-pda<sup>2-</sup> ligands in the apical positions. The pyrazine nitrogen atom N1 and tetrazole nitrogen atom N3 of 2-pztz coordinate to the Co(II)

center in a chelating mode and the resulting Co(2-pztz)<sup>2+</sup> complex cations are in turn connected by the nitrogen atom N4 (adjacent to nitrogen atom N3) of the tetrazole ring to form a six membered dimer ring with a Co–Co separation of 4.179 Å. The overall connectivity of the 2-pztz<sup>1-</sup> ligands to the metal centers results in the formation of Co-dimer {Co<sub>2</sub>(2-pztz)<sub>2</sub>} rings as shown in Fig. 5b. The 2-pztz<sup>1-</sup> in the crystal structure exhibits a μ<sub>3</sub> coordination mode (μ<sub>2</sub> from tetrazole ring and μ<sub>1</sub>

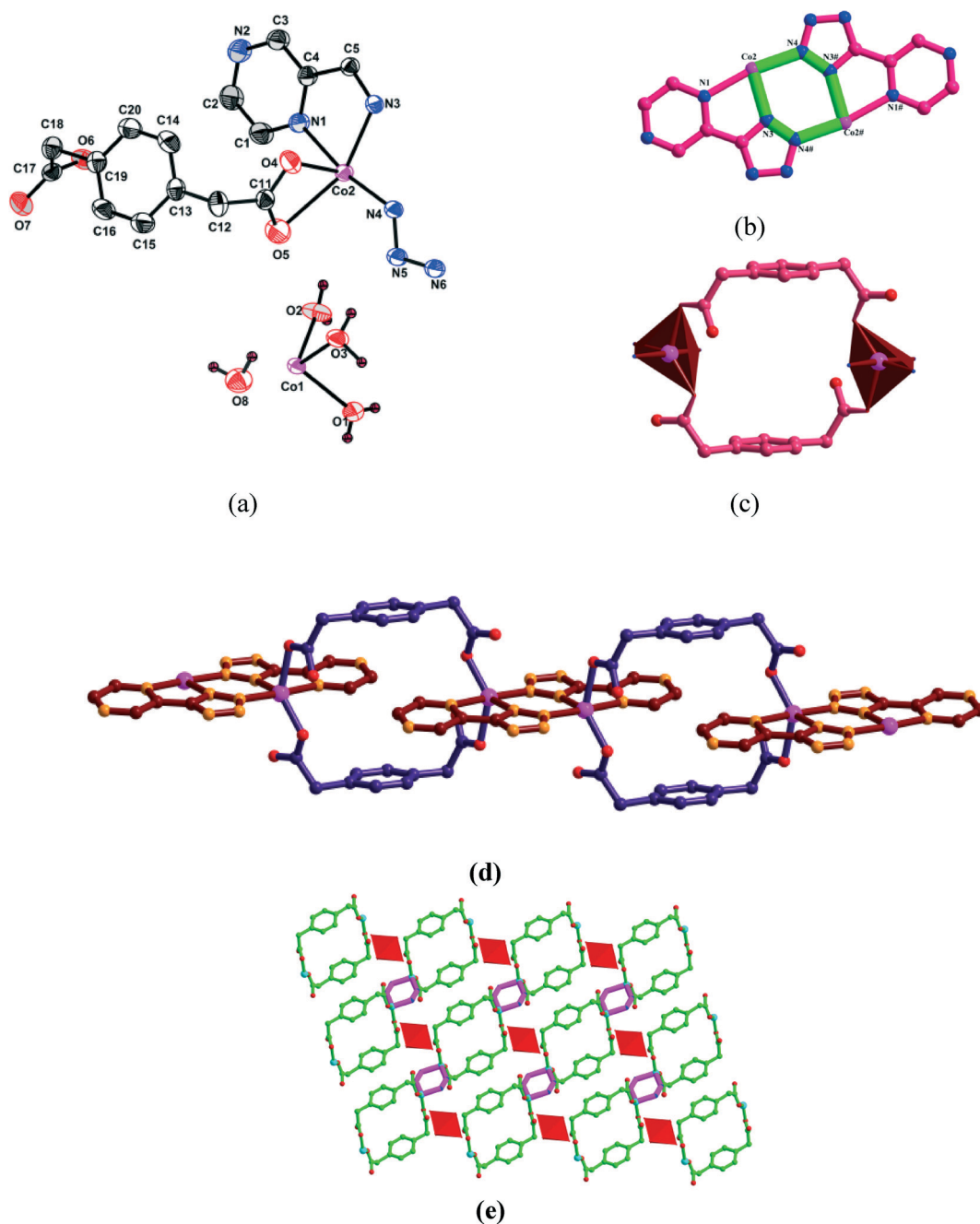


**Fig. 5** (a) ORTEP view of the basic unit of **4a**. Hydrogen atoms of carbon atoms have been removed for clarity. Thermal ellipsoids are at the 30% probability level. (b) Co-dimer ring formed due to chelated connectivity of 2-pztz<sup>1-</sup>. (c) Molecular loop formed due to *cis* connectivity of the 1,4-pda<sup>2-</sup> ligand. (d) 1D extended chain formed due to connectivity of 2-pztz and 1,4-pda ligands (e) 2D packing diagram illustrating the position of cationic species in the cavities.

from pyrazine ring) and the other nitrogen atom N2 in the pyrazine ring remains uncoordinated. The  $\{Co_2(2-ptz)_2\}$  dimer connects to other dimers through two pairs of 1,4-pda<sup>2-</sup> ligands in a typical *cis* conformation. Each 1,4-pda<sup>2-</sup> coordinates to the metal center through the  $\mu_1$  coordination mode and the acetate side chains in the skeleton are twisted with respect to each other through a synclinal torsion angle of 49.06 Å (viewed through C11–C12–C17–C18) indicating a typical *cis* conformation. The presence of 1,4-pda<sup>2-</sup> in the *cis* conformation results in the formation of  $\{Co_2(1,4-pda)_2\}$  molecular loops as shown in Fig. 5c. Overall, the connectivity of these loops with the dimers results in the formation of a 1D extended chain along the crystallographic *c* axis as shown in Fig. 5d. The hexa aqua cobalt(II) cations compensate the charge of the anionic chains by staying as a lattice component. From the crystal packing diagram,  $[Co(H_2O)_6]^{2+}$  cations are located between the two adjacent chains along the plane and nearly sandwiched between the two  $\{Co_2(1,4-pda)_2\}$  loops along with the lattice water molecules (Fig. 5e). As anticipated, due to the presence of lattice water molecules and coordinated water molecules in the hexa aqua cationic complex, strong hydrogen bonding was expected. The four coordinated water molecules in each  $[Co(H_2O)_6]^{2+}$  cation are hydrogen bonded to carboxylate oxygen atoms of 1,4-pda<sup>2-</sup> moieties of four anionic 1D chains and two lattice water molecules through O–H...O interactions.

$[Co_2(\mu-OH)(1,3-pda)(4-ptz)]_n$  (**4b**) and  $[Co_2(\mu-OH)(1,4-pda)(4-ptz)]_n \cdot nH_2O$  (**4c**). Both compounds crystallize in the monoclinic space group  $P2_1/n$ . The compounds **4b** and **4c** are isostructural except the carboxylate ligand 1,3-pda in **4b** is replaced by 1,4-pda in **4c** and a lattice water molecule is present in compound **4c**, which is absent in compound **4b**. The structural description of compound **4c** was elucidated in our previous report,<sup>8</sup> herein, we describe the structural description of **4b** and the structural consequences obtained by replacing 1,4-H<sub>2</sub>pda with 1,3-H<sub>2</sub>pda in terms of torsion angles and length of the ligand, *etc.* The asymmetric unit of compound **4b** consists of two Co(II) atoms in tbp geometry connected by the  $\mu_2$ -hydroxy group and one 1,3-pda<sup>2-</sup> and 4-ptz<sup>1-</sup> anion (Fig. 6a). Both the acetate groups in the 1,3-pda<sup>2-</sup> anion adopt  $\mu_2-\eta_{1,1}$  coordination modes in a typical *cis* conformation with a synclinal torsion angle of 29.84° (viewed through C8–C7–C9–C10), to form a metallo macrocycle, whereas the torsion angle exhibited by the acetate side chains of 1,4-pda<sup>2-</sup> in compound **4b** is perfectly *cis* with a synclinal torsion angle of 2.30 Å. The major structural changes observed in the metalocycles are formed due to the *cis* connectivity of the carboxylate ligands, *i.e.* a 22-membered macrocycle with dimensions of  $7.531 \times 8.109 \text{ Å}^2$  was observed in the case of 1,4-pda<sup>2-</sup> whereas a 20-membered macrocycle with dimensions of  $8.322 \times 7.946 \text{ Å}^2$  was formed in the case of the 1,3-pda<sup>2-</sup> associated compound. Also, the benzene rings of pda<sup>2-</sup> in the metalocycle formed in compound **4c** are faced parallel to each other due to 1,4-connectivity in the pda<sup>2-</sup> ligand, but the benzene rings are not faced parallel to each other in compound **4b** due to 1,3-connectivity in the pda<sup>2-</sup> ligand (Fig. 6b). The 20 membered macrocycle, formed in **4b** extends its dimensionality with four other macrocycles through the bridging hydroxyl

group ( $\mu_2$ -OH) to form a 2D network (Fig. 6c). The co-ligand ptz in  $\mu_4$  coordination mode ( $\mu_3$  from the tetrazole ring and  $\mu_1$  from the pyridine ring of the ptz) again connects this 2D network. The connectivity of the tetrazole to the Co(II) centres results in the formation of a 1D chain in which the adjacent Co(II) ions are bridged by the nitrogen atoms of the tetrazole ring and  $\mu_2$ -OH groups. The connectivity of pda<sup>2-</sup> in a *cis* conformation results in the formation of macrocycles which extend their dimensionality by bridging with  $\mu_2$ -OH groups and the tetrazole ring to form 2D layers as shown in Fig. 6d.

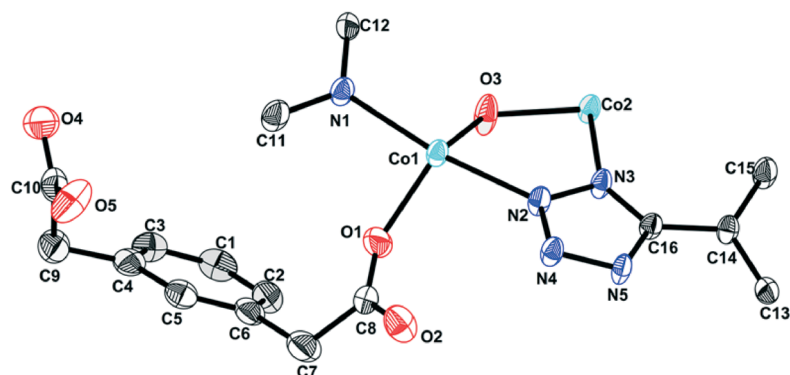
### Role of linker coordination angle

Scheme 1 displays the possible LCAs of the phenylenediacetates, isomeric bis(imidazole-1-ylmethyl)-benzene linkers, bent carboxylate ligand hfipbb<sup>2-</sup>, bent flexible carboxylate linker ADA<sup>2-</sup> and rigid tetrazoles. The combination of these linkers in constructing mixed linker coordination networks can often lead to intriguing dimensionalities. The compounds discussed in this study are present under four different classes to demonstrate the rational affect of the linker coordination angle.

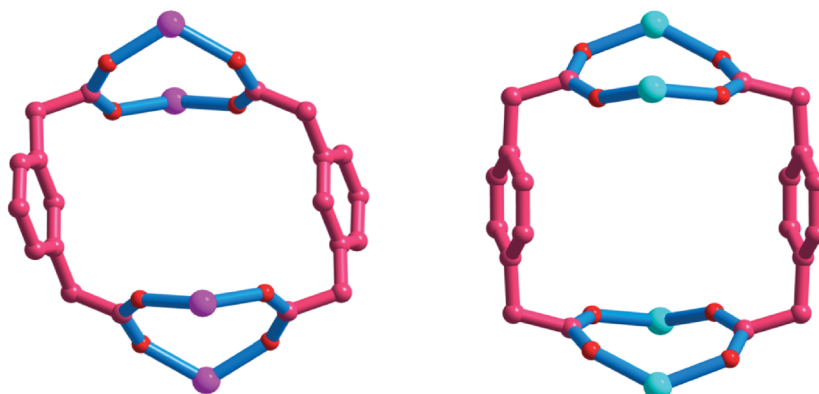
#### (Flexible, flexible)

In this section, the two compounds **1a** and **1b** were synthesized with a mixed (flexible, flexible) linkers system. As shown in Scheme 2, the connectivity of 1,2-pda and 1,2-bix results in the formation of 2D layers in compound **1a** and the connectivity of 1,4-pda and 1,4-bix results in the formation of a 3D framework in compound **1b**. In both compounds, the Co(II) ion is present in the same  $\{CoN_2O_4\}$  tetrahedral geometry, but the linker coordination angle (LCA) changes the dimensionality of the compounds. In compound **1a**, the LCAs of both the ligands are 60° whereas, the LCAs of the ligands in compound **1b** are 180°. The difference in these LCAs changes the length of the linker, resulting in changes in the annex of the linker. The linker with the lowest LCA generally creates the minimum separation between the metal polyhedra. The separation created by the 1,2-pda and 1,2-bix ligands in compound **1a** is 8.512 Å and 12.114 Å, respectively, while the separation created by the 1,4-pda and 1,4-bix ligands in compound **1b** is 12.80 Å and 15.09 Å. Due to the longer length, the ligands protrude outside the layer to form a 3D framework, whereas, the short linkers connect to the metal centres in the same layer.

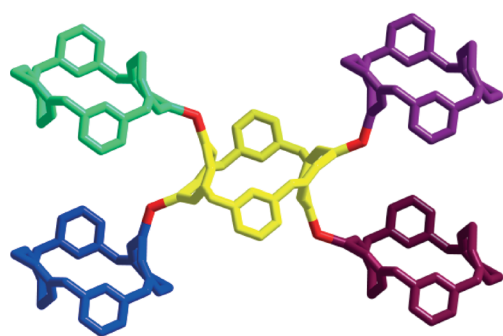
In both compounds, the carboxylate ligands (1,2-pda and 1,4-pda) and N-donor secondary ligands (1,2-bix and 1,4-bix) adopt a *trans* conformation. The flexibility of the linkers is one of the reasons of why the longer ones protrude outside the 2D plane to form a 3D structure (**1b**) and the shorter ones remain in the same plane (**1a**). Compounds **1a** and **1b** are mixed linker coordination networks in which both the linkers exhibit the same LCA values, *i.e.* either 60° and 60° in **1a** or 180° and 180° in **1b**. Perhaps in this system, the lower LCAs form 2D structures and the higher LCAs form 3D structures and the linkers with mixed LCAs form either 2D or 3D only.



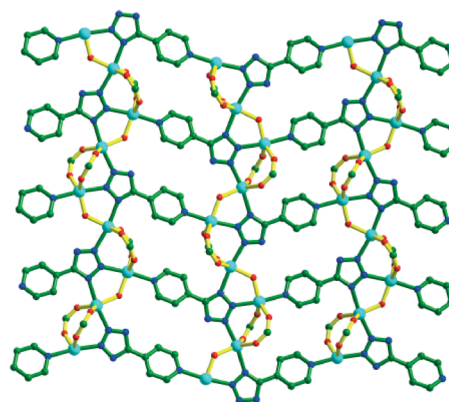
(a)



(b)



(c)



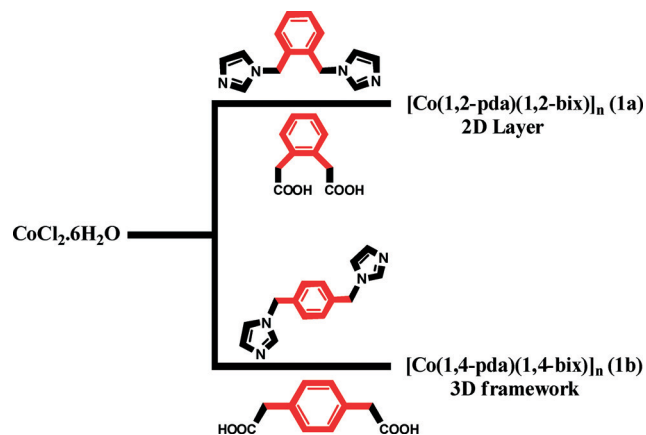
(d)

**Fig. 6** (a) ORTEP view of the basic unit of **4b**. Hydrogen atoms of carbon atoms have been removed for clarity. Thermal ellipsoids are at the 40% probability level. (b) Molecular box formed due to the *cis* conformation of the  $\text{pda}^{2-}$  ligand (left for 1,3- $\text{pda}^{2-}$  in **4b** and right for 1,4- $\text{pda}^{2-}$  in **4c**). (c) Four connectivity extension of molecular boxes through the  $\mu_2$ -OH group. (d) Overall 2D network of compound **4b** (phenylene rings of 1,3- $\text{pda}^{2-}$  are omitted for clarity).

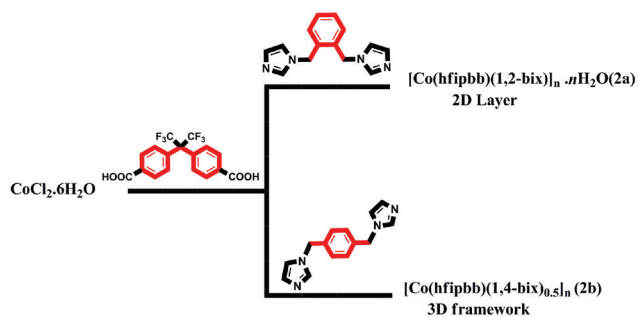
### (Bent, flexible)

In this section, the two compounds **2a** and **2b** with a (bent, flexible) mixed linker system are discussed. As shown

in Scheme 3, the compounds **2a** and **2b** are constituted by a Co-hfipbb-(1,*n*)-bix (*n* = 2,4) composition matrix. Compound **2a** is a 2D structure and **2b** is a 3D layered-pillared framework. Both the compounds contain metal-hfipbb architectures which



**Scheme 2** Affect of dimensionality by changing the linker coordination angle of the isomeric bis(imidazole-1-ylmethyl)-benzene (bix) ligands and phenylene diacetate (pda) ligands.



**Scheme 3** Affect of dimensionality by changing the linker coordination angle of the isomeric bis(imidazole-1-ylmethyl)-benzene (bix) ligands with the metal-hfipbb system.

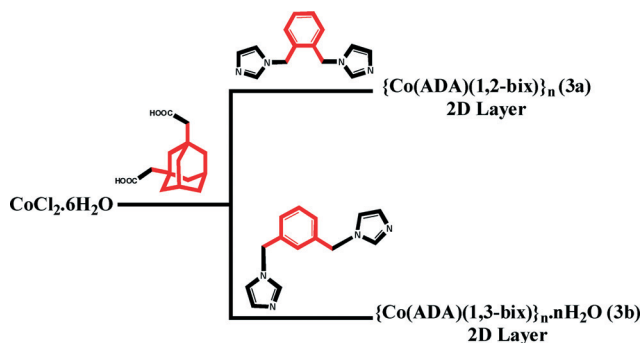
are extended by bix linkers. In compound 2a, metal-hfipbb forms 1D chains, which are connected by 1,2-bix ligands to form 2D layers whereas in 2b, metal-hfipbb forms 2D helical double layers which are connected by 1,4-bix to form a 3D layered-pillared framework. The linker coordination angles of 1,2-bix and 1,4-bix are  $60^\circ$  and  $180^\circ$ , respectively; as a result, the length of the ligands in the crystal structures are  $7.75 \text{ \AA}$  and  $11.21 \text{ \AA}$ , respectively. In both compounds, the bix linker adopts a *trans* conformation with variable torsion angles ( $151.84^\circ$  for 2a, and  $180^\circ$  for 2b). The longer 1,4-bix favors the formation of metal-carboxylate paddlewheel layers in compound 2b, since its length can separate these layers with a definite distance to reduce the intermolecular repulsions. However the shorter 1,2-bix does not favor the formation of paddlewheels, as a result the metal-hfipbb forms 1D chains. In our previous report,<sup>11a</sup> the steric hindrance created by a secondary linker at the coordination sphere for the formation of paddlewheels was studied. From these two examples, it can be correlated that the formation of paddlewheels would be more favorable with longer secondary linkers. In fact, this observation is in accordance with other systems with longer linkers, e.g., 1,2-dpe, bpy as found in the literature.<sup>19</sup>

### (Bent flexible, flexible)

In this section, we tried to rationalize the effect of LCA on the (bent flexible, flexible) mixed linker system. We chose the 1,3-positioned adamantane diacetate linker with a LCA of  $120^\circ$  which also includes flexibility in its geometry. The associated connectivity of  $\text{ADA}^{2-}$  with flexible bix linkers results in interesting topologies which differ from the expected ones. Both the compounds are 4,4 connected 2D layers but the topology in both cases are different from each other. In compound 3a, the 1,2-bix linker with a LCA of  $60^\circ$  exists in the *cis* conformation and creates a large separation of  $13.648 \text{ \AA}$  between the two metal centers, but interestingly the 1,3-bix linker with a LCA of  $120^\circ$  exists in the *trans* conformation and creates a separation of  $11.146 \text{ \AA}$  between the two Co(II) centers in 3b. Usually 1,3-bix in a *trans* conformation creates a larger separation than 1,2-bix in the *cis* conformation, but the opposite is observed in the case of compounds 3a and 3b. The main advantage of flexible linkers is that they can modulate their length according to the available coordination configurations by modulating their conformations. In this case, the coordination restrictions, imposed by the  $\text{ADA}^{2-}$  in compounds 3a and 3b, dictates the geometrical parameters of the bix linkers. In the case of compound 3a,  $\text{ADA}^{2-}$  forms a 1D zig-zag chain with left and right turns, whereas  $\text{ADA}^{2-}$  forms a 1D linear chain in 3b. The connectivity of these 1D chains with the bix linker forms different topologies; in the case of 1,2-bix, two different parallelograms are formed in the 2D layer and in the case of 1,3-bix, parallelograms with unique dimensions are formed in the 2D layer. This difference in the skeleton of the 2D sheets can be correlated with the geometrical parameters exposed by the bix linkers (Scheme 4).

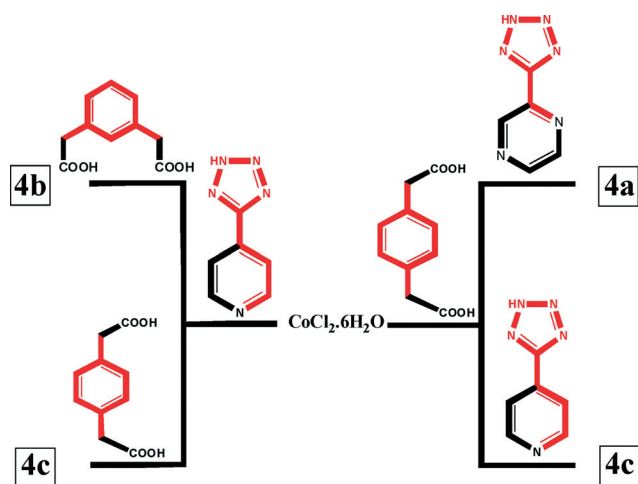
### (Flexible, rigid)

In this section, compounds 4a, 4b and 4c in a (flexible, rigid) mixed linker system are considered. The important parameter in this discussion (for this type of mixed linker system) is the rigid secondary linker. The flexible primary linker always



**Scheme 4** Influence of LCA of secondary bix linker on modulating the topology of 2D layers in isomeric bis(imidazole-1-ylmethyl)-benzene (bix) ligands in the metal-ADA system.

adopts a *cis* conformation. As shown in Scheme 5, both compounds **4b** and **4c** are isostructural, even though the LCAs of the carboxylate linkers are 180° in **4b** and 120° in **4c**. In both these compounds, the flexible carboxylate ligands adopt a *cis* conformation which primarily decreases the dimensionality. Usually *cis* conformations form low dimensional structures whereas *trans* conformations form high dimensional structures. In this scenario, the other factor, *i.e.* the LCA of the secondary linker, plays an important role in tuning the dimensionality. In compounds **4a** and **4b** the secondary linker is 4-ptz with a LCA of 180°; as a result, both these compounds are 2D iso-structural compounds. Whereas in **4a**, when 1,4-pda adopts a *cis* conformation, a 1D chain is formed, this is because the secondary ligand 2-tzpz has an LCA of 60°. In the case of tetrazole linkers, the LCA was measured between the tetrazole ring and the position of the nitrogen atom in the pyridine ring. When the LCA is 60°, the skeleton of the tetrazole resembles 2,2'-bipyridine and adopts a chelated coordination mode thereby blocking the two coordination sites of Co(II) centers, which results in the lower dimensional compound **4a**; the *cis* conformation of 1,4-pda also favors the formation of a 1D chain, as observed in the case of **4a**. We tried to rationalize this effect with 2-ptz with a LCA of 60°, but we were unable to synthesize a 2-ptz-1,4-pda assembled compound, so we chose 2-tzpz which has two LCAs: 60° and 120°, and fortunately in the crystal structure of **4a**, 2-tzpz utilizes only the LCA of 60° which helps us to elucidate the affect of the LCA. Overall, in the mixed linker (flexible, rigid) system, where the flexible linker adopts a *cis* conformation, the LCA of the secondary linker decides the dimensionality of the final architectures. Also from these three examples, the (flexible, rigid) system always forms a 2D or 1D dimensional structure instead of higher dimensionality 3D systems. The overall structural outcomes are tabulated in Table 3.



**Scheme 5** Affect of dimensionality by changing the linker coordination angle of the isomeric phenylenediacetate ligands with different rigid tetrazole ligands.

**Table 3** The structural outcomes of all the compounds presented in this study

Compound	LCA (acid, N-donor)	Mixed linker type <sup>a</sup>	Dimensionality
<b>1a</b>	60,60	F,F	2D
<b>1b</b>	180,180	F,F	3D
<b>2a</b>	120,60	B,F	2D
<b>2b</b>	120,180	B,F	3D
<b>3a</b>	120,60	BF,R	2D
<b>3b</b>	120,120	BF,R	2D
<b>4a</b>	180,60	F,R	1D
<b>4b</b>	120,180	F,R	2D
<b>4c</b>	180,180	F,R	2D

<sup>a</sup> F = Flexible, B = Bent, BF = Bent flexible, R = Rigid.

### PXRD and thermogravimetric analysis

To ensure the phase purity of the compounds, presented in this study, powder X-ray diffraction (PXRD) patterns of the powder samples were recorded. The diffraction patterns for the simulated data (calculated from single crystal data) matched well with the observed data which proves the bulk homogeneity of the crystalline solids (see section 3 of ESI† for the PXRD patterns). The experimental patterns have a few un-indexed diffraction peaks and some are slightly broadened and shifted in comparison to the simulated patterns but still it can be regarded that the bulk as-synthesized materials represent the compounds.

TGA plots were recorded under flowing N<sub>2</sub> for crystalline samples of the title compounds in the temperature range 40–1000 °C (see relevant plots in section-4, ESI†). Compound **1a** is stable up to 296 °C and undergoes a steep weight loss up to 402 °C followed by a continuous weight loss up to 1000 °C with a residual mass of 29.3%. Compound **2a** loses one crystalline water with a weight loss of 2.63% (theoretical weight loss 2.5%) in the temperature region of 40 °C to 115 °C and the network remains stable up to 295 °C. The dehydrated network undergoes a sharp weight loss up to 455 °C and then undergoes continuous weight loss up to 1000 °C. The thermogravimetric curves of compounds **3a** and **3b** follow the same pathway, as both compounds are stable up to 350 °C followed by decomposition of the associated organic moieties in two steps at 475 °C and 535 °C with gradual weight loss up to 1000 °C. Compound **4a** remains stable up to 100 °C and loses six coordinated water molecules of [Co(H<sub>2</sub>O)<sub>6</sub>]<sup>2+</sup> and two solvent water molecules in the temperature region of 100 °C to 225 °C with a weight loss of 14.9% (theoretical 14.4%); the dehydrated compound remains stable up to 306 °C and undergoes continuous weight loss up to 1000 °C. Compound **4b** is thermally stable up to 350 °C and undergoes a weight loss continuously in two steps at higher temperatures.

### Electronic absorption properties

Solid state diffuse reflectance spectra for all compounds were measured in the region 200–800 nm (the relevant spectra are presented in section 5 of the ESI†). The absorption maxima

at higher wavelengths 547 nm, 574 nm (for **1a**), 529 nm, 581 nm (for **2a**), 529 nm, 590 nm (for **3a**) 523 nm, 585 nm (for **3b**), 527 nm for **4a** and 522 nm for **4b** are tentatively assigned to d-d transitions in the  $d^7$  Co(II) ion. The energy bands, observed at lower wavelengths in their electronic absorption spectra, are due to  $\pi-\pi^*$  transitions from the phenyl rings which are comparable with the transitions observed in the free ligands.

## Magnetic properties

### Compound 2a

The magnetic properties of compound **2a**, as plots of  $\chi_M T$  vs.  $T$  and  $\chi_M$  vs.  $T$  are shown in Fig. 7a. The  $\chi_M T$  value at room temperature (300 K) is  $2.40 \text{ cm}^3 \text{ K mol}^{-1}$ , which is much higher than the expected value for an isolated Co<sup>II</sup> ion ( $\chi_M T = 1.875 \text{ cm}^3 \text{ K mol}^{-1}$  for a  $S = 3/2$  ion). The  $\chi_M T$  value decreases gradually to  $1.31 \text{ cm}^3 \text{ K mol}^{-1}$  at 2 K.  $1/\chi_M$  vs.  $T$  follows the Curie Weiss law in the temperature range 2–300 K with a negative Weiss constant  $\theta = -5.23 \text{ K}$  and  $C = 2.403 \text{ cm}^3 \text{ K mol}^{-1}$ . The higher value of  $\chi_M T$  indicates spin-orbit coupling of the tetrahedral Co(II) ion, which can be estimated by the zero-field splitting (ZFS) effects of a single-ion of Co(II).

The  $\chi_M$  data in the temperature range 2–300 K was fitted by the following expressions for  $S = 3/2$  systems with dominant zero field splitting effects,  $D,^{22}$  (eqn (1)–(4)):

$$\chi_{\parallel} = (Ng^2\beta^2/KT)[A/B] \quad (1)$$

where  $A = [1 + 9\exp(-2D/KT)]$  and  $B = [4(1 + \exp(-2D/KT))]$

$$\chi_{\perp} = (Ng^2\beta^2/KT)[C/D] \quad (2)$$

where  $C = [4 + (3KT/D)(1 - \exp(-2D/KT))]$  and  $D = [4(1 + \exp(-2D/KT))]$ .

$$\chi_M' = [(\chi_{\parallel} + \chi_{\perp})/3] \quad (3)$$

$$\chi_M = \chi_M' / \{1 - \chi_M'(2zJ'/Ng^2\beta^2)\} \quad (4)$$

The parameters  $N$ ,  $\beta$  and  $K$  have their normal meanings. The best fit was obtained from 2–300 K with  $g = 2.27$  (2)  $D = -6.07$  (1)  $\text{cm}^{-1}$  and  $zJ' = 2.49$  (6) with a agreement factor of  $1.82 \times 10^{-4}$ . The value of  $D$ , calculated from the above expressions is in the range expected for a tetrahedral metal center (*i.e.*  $D = -36$  to  $+13 \text{ cm}^{-1}$ ).<sup>22b</sup>  $D = -6.07 \text{ cm}^{-1}$  indicates a  $2D = 12.14 \text{ cm}^{-1}$  splitting between the ground  $M_S = \pm 3/2$  levels and the excited  $M_S = \pm 1/2$  levels.

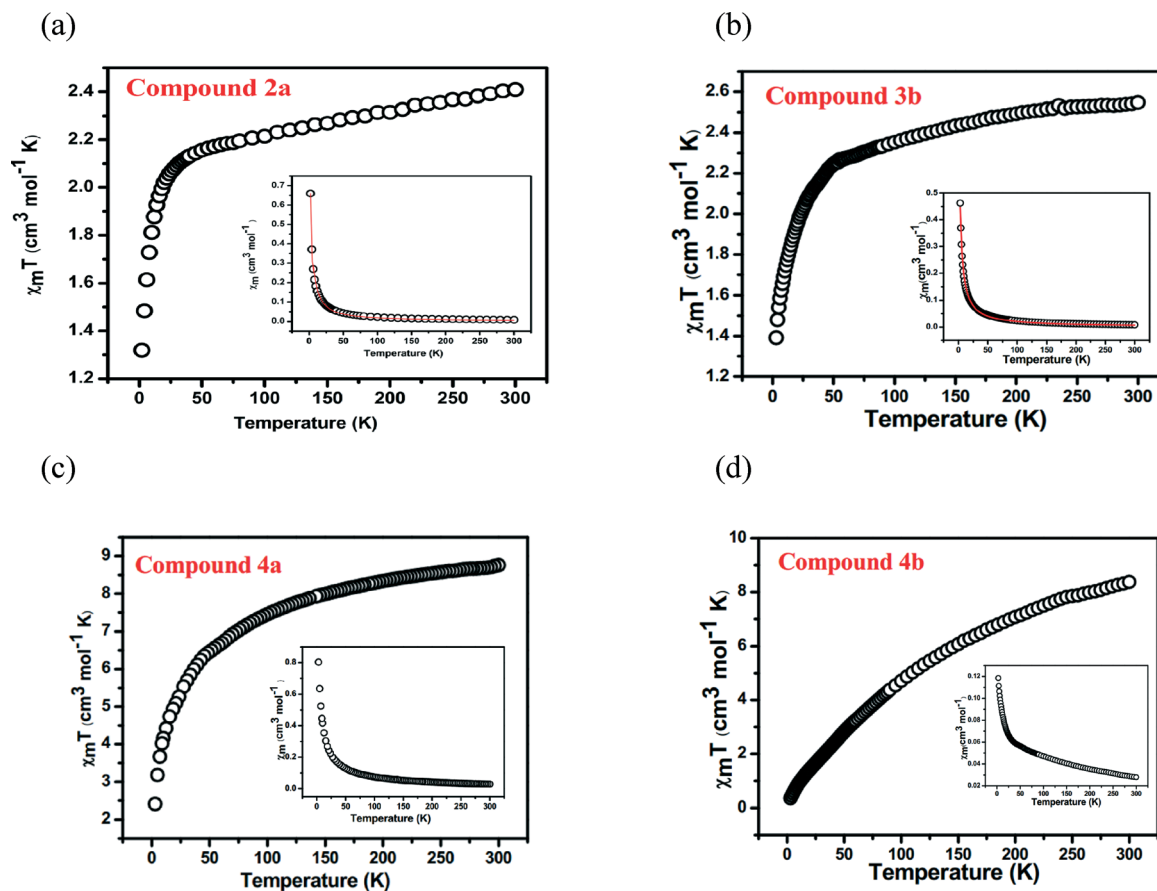


Fig. 7 Plots of  $\chi_M T$  vs.  $T$  and  $\chi_M$  vs.  $T$  (inset) for the compounds **2a**, **3b**, **4a** and **4b** in the temperature range of 2–300 K. The red line indicates fitting using the theoretical model (see text).

### Compound 3b

The magnetic properties of compound **3b** are roughly the same magnetic properties as compound **2a**. The plots of  $\chi_M T$  vs.  $T$  and  $\chi_M$  vs.  $T$  for compound **3b** in the temperature range 2–300 K are shown in Fig. 7b. The  $\chi_M T$  value at room temperature is  $2.54 \text{ cm}^3 \text{ K mol}^{-1}$  which is higher than that of compound **3b** and it decreases slowly down to 2 K ( $1.39 \text{ cm}^3 \text{ K mol}^{-1}$ ). The Curie Weiss fitting reveals a value of  $\theta = -7.4 \text{ K}$  and  $C = 2.5 \text{ cm}^3 \text{ K mol}^{-1}$ , indicating the antiferromagnetic nature of the compound. The observed spin-orbit coupling was estimated by the zero-field splitting (ZFS) effects using the same equation as mentioned above. The best fitting of  $\chi_M$  vs.  $T$  data in the temperature range 2–300 K gave  $g = 2.27$  (2)  $D = -8.45$  (1)  $\text{cm}^{-1}$  and  $zJ' = 3.62$  (4). The higher  $D$  value indicates the larger splitting between the  $M_S = \pm 3/2$  levels and  $M_S = \pm 1/2$  levels compared to compound **2a**.

### Compound 4a

Both  $\chi_M$  vs.  $T$  and  $\chi_M T$  vs.  $T$  plots of compound **4a** are presented in Fig. 7c. The room temperature  $\chi_M T$  value of compound **4a** is  $8.76 \text{ cm}^3 \text{ K mol}^{-1}$  which is much higher than the spin only value of  $5.625 \text{ cm}^3 \text{ K mol}^{-1}$  for the three Co(II) ions ( $S = 3/2$  and  $g = 2$ ) indicating an unquenched orbital contribution of the Co(II) ion. By lowering the temperature, the  $\chi_M T$  value continuously decreases to  $2.41 \text{ cm}^3 \text{ K mol}^{-1}$  at 2 K. The data follow the Curie Weiss law with the Weiss constant  $\theta = -20 \text{ K}$  agreeing with the antiferromagnetic behavior of the compound, reflecting a plausible antiferromagnetic interaction between the two Co(II) ions in the dimer through N atoms of the tetrazole ring. In compound **4a** the two Co(II) ions are bridged by the nitrogen atoms of the tetrazole ring and the remaining Co(II) atom is in the lattice position of a perfect octahedron. This factor makes it difficult to analyze the exchange phenomenon through the bridge. Because of the lack of a suitable model for such a system, fitting of the magnetic susceptibility and the relevant exchange parameters could not be estimated.

### Compound 4b

The investigation of the magnetic study of compound **4b** in the temperature range 2–300 K reveals that the  $\chi_M T$  value at room temperature is  $8.37 \text{ cm}^3 \text{ K mol}^{-1}$  which is much more higher than the spin only value ( $3.75 \text{ cm}^3 \text{ K mol}^{-1}$ ) for two Co(II) ions ( $S = 3/2$  and  $g = 2$ ). As the temperature is lowered, there is a continuous sharp decrease in the  $\chi_M T$  value which reaches a minimum value of  $0.35 \text{ cm}^3 \text{ K mol}^{-1}$  at 2 K. The data of the  $\chi_M$  vs.  $T$  and  $\chi_M T$  vs.  $T$  plots (Fig. 7d) indicates the strong antiferromagnetic exchange between neighboring Co(II) metal ions. The strong antiferromagnetic exchange is also supported by the high Weiss constant  $\theta = -160 \text{ K}$ . As described in the crystal structure of the compound **4b**, a 1D chain is formed by the connectivity of the Co(II) ions bridged by double carboxylate bridges, a hydroxo bridge, tetrazolate  $N_2$  and tetrazolate  $N_3$  bridge. The magnetostucture of the compound contains many pathways for magnetic interaction;

the lack of a proper model for such a system makes it difficult to estimate the exchange parameters for this compound.

## Conclusion

In designing coordination polymers based on flexible linkers, several factors influence the self-assembly process; among those, the angle between the position of the coordinating groups, *i.e.* the linker coordination angle (LCA), is an important factor that alters the dimensionality and topology of the coordination networks. This concept has been discussed elaborately in this article taking a series of compounds, based on flexible linkers having intriguing skeletons. The self-assembly of a (flexible, flexible) mixed linker system reveals the amendment of dimensionality according to the length of the linker, which is dependent on LCA. The formation of the Co-hfipbb matrix as a 1D chain in **2a** and a 2D interpenetrated double layer in **2b**, assisted by the secondary N-donor bix linkers having LCAs of  $60^\circ$  (for **2a**), and  $180^\circ$  (for **2b**) reveals the essential role of the position of the coordinating groups on the linker. The associated connectivity of the Co-ADA matrix with secondary N-donor bix linkers having LCAs of  $60^\circ$  (for **3a**), and  $120^\circ$  (for **3b**) results in the formation of 2D layers with different topologies. Compounds **4a**, **4b** and **4c** are coordination networks based on {M-pda-tz} constituents in which the flexible carboxylates 1,4-pda in **4a** and **4c** and 1,3-pda in **4b** adopt a *cis* conformation which have the same structural consequences on the dimensionality; in this situation, the LCA of the tetrazole directs the dimensionality in obtaining 2D structures in **4b** and **4c** with tetrazole LCAs of  $180^\circ$  and a 1D structure for **4a** with a tetrazole LCA of  $60^\circ$ . All the compounds discussed in the study are a series of examples to enrich the structural library of coordination networks based on flexible linkers exploiting the role of linker coordination angle. Finally the temperature dependent magnetic susceptibility measurements divulge the zero-field splitting parameters of compounds **2a** and **3b** and the antiferromagnetic exchange interactions between the metal centers in **4a** and **4b**.

## Acknowledgements

The authors thank the Science & Engineering Research Board (a statutory body under the Department of Science and Technology, Government of India) for financial support (project number SB/S1/IC/034/2013). The National X-ray Diffractometer facility at the University of Hyderabad by the Department of Science and Technology, Government of India, is gratefully acknowledged. We are grateful to UGC, New Delhi, for providing infrastructure facility at University of Hyderabad under UPE grant. BKT and PM thank CSIR, India for their fellowships.

## References

- (a) S. R. Halper, L. Do, J. R. Stork and S. M. Cohen, *J. Am. Chem. Soc.*, 2006, **128**, 15255; (b) S. Hasegawa, S. Horike, R. Matsuda, S. Furukawa, K. Mochizuki, Y. Kinoshita and

- S. Kitagawa, *J. Am. Chem. Soc.*, 2007, **129**, 2607; (c) S. Kitagawa and R. Matsuda, *Coord. Chem. Rev.*, 2007, **251**, 2490; (d) O. M. Yaghi, M. O'Keeffe, N. W. Ockwig, H. K. Chae, M. Eddaoudi and J. Kim, *Nature*, 2003, **423**, 705; (e) F. Luo, J. M. Zheng and S. R. Batten, *Chem. Commun.*, 2007, 3744.
- 2 (a) R. Kitaura, K. Fujimoto, S. Noro, M. Kondo and S. Kitagawa, *Angew. Chem., Int. Ed.*, 2002, **41**, 133; (b) D. M. Shin, I. S. Lee and Y. K. Chung, *Inorg. Chem.*, 2003, **42**, 8838; (c) P. Ayappan, O. R. Evans, Y. Cui, K. A. Wheeler and W. B. Lin, *Inorg. Chem.*, 2002, **41**, 4978; (d) M. Dinca and J. R. Long, *J. Am. Chem. Soc.*, 2005, **127**, 9376; (e) B. Bhattacharya, R. Dey, P. Pachfule, R. Banerjee and D. Ghoshal, *Cryst. Growth Des.*, 2013, **13**, 731; (f) D. Ghoshal, G. Mostafa, T. K. Maji, E. Zangrando, T.-H. Lu, J. Ribas and N. R. Chaudhuri, *New J. Chem.*, 2004, **28**, 1204.
- 3 (a) A. Schaate, S. Klingelhofer, P. Behrens and M. Wiebcke, *Cryst. Growth Des.*, 2008, **8**, 3200; (b) Y. Liu, Y. Qi, Y. Y. Lv, Y. X. Che and J. M. Zheng, *Cryst. Growth Des.*, 2009, **9**, 4797; (c) Z. X. Li, T. L. Hu, H. Ma, Y. F. Zeng, C. J. Li, M. L. Tong and X. H. Bu, *Cryst. Growth Des.*, 2010, **10**, 1138; (d) J. Yang, J. F. Ma, S. R. Batten and Z. M. Su, *Chem. Commun.*, 2008, 2223.
- 4 J.-R. Li and H.-C. Zhou, *Angew. Chem., Int. Ed.*, 2009, **48**, 8465.
- 5 (a) A. J. Blake, N. R. Champness, S. S. M. Chung, W. S. Li and M. Schröder, *Chem. Commun.*, 1997, 1005; (b) M. Maekawa, H. Konaka, Y. Suenaga, T. K. Sowa and M. Munakata, *J. Chem. Soc., Dalton Trans.*, 2000, 4160; (c) H. C. Wu, P. Thanasekaran, C. H. Tsai, J. Y. Wu, S. M. Huang, Y. S. Wen and K. L. Lu, *Inorg. Chem.*, 2006, **45**, 295; (d) B. Y. Cho, D. Min and S. W. Lee, *Cryst. Growth Des.*, 2006, **6**, 342.
- 6 (a) A. J. Blake, N. R. Brooks, N. R. Champness, M. Crew, A. Deveson, D. Fenske, D. H. Gregory, L. R. Hanton, P. Hubberstey and M. Schroder, *Chem. Commun.*, 2001, 1432; (b) S. Sanda, S. Parshamoni, A. Adhikary and S. Konar, *Cryst. Growth Des.*, 2013, **13**, 5442; (c) S. Sanda, S. Parshamoni and S. Konar, *Inorg. Chem.*, 2013, **52**, 12866.
- 7 (a) G. Li, J. Lu, X. Li, H. Yang and R. Cao, *CrystEngComm*, 2010, **12**, 3780; (b) T. F. Liu, J. Lu, X. Lin and R. Cao, *Chem. Commun.*, 2010, **46**, 8439; (c) X. Li, X. Weng, R. Tang, Y. Lin, Z. Ke, W. Zhou and R. Cao, *Cryst. Growth Des.*, 2010, **10**, 3228; (d) Z.-J. Lin, Y.-B. Huang, T.-F. Liu, X.-Y. Li and R. Cao, *Inorg. Chem.*, 2013, **52**, 3127; (e) Z.-J. Lin, L.-W. Han, D.-S. Wu, Y.-B. Huang and R. Cao, *Cryst. Growth Des.*, 2013, **13**, 255; (f) Z.-J. Lin, T.-F. Liu, Y.-B. Huang, J. Lü and R. Cao, *Chem.-Eur. J.*, 2012, **18**, 7896; (g) Z.-J. Lin, T.-F. Liu, X.-L. Zhao, J. Lü and R. Cao, *Cryst. Growth Des.*, 2011, **11**, 4284.
- 8 B. K. Tripuramallu, P. Manna, S. N. Reddy and S. K. Das, *Cryst. Growth Des.*, 2012, **12**, 777.
- 9 T. Liu, J. Lu, L. Shi, Z. Guo and R. Cao, *CrystEngComm*, 2009, **11**, 583.
- 10 G. P. Yang, Y. Y. Wang, W. H. Zhang, A. Y. Fu, R. T. Liu, E. Lermontava and Q. Z. Shi, *CrystEngComm*, 2010, **12**, 1509.
- 11 (a) P. Manna, B. K. Tripuramallu and S. K. Das, *Cryst. Growth Des.*, 2012, **12**, 4607; (b) B. K. Tripuramallu, S. Mukherjee and S. K. Das, *Cryst. Growth Des.*, 2013, **13**, 2426; (c) P. Manna, B. K. Tripuramallu and S. K. Das, *Cryst. Growth Des.*, 2014, **14**, 278.
- 12 (a) L. Pan, K. M. Adams, H. E. Hernandez, X. Wang, C. Zheng, Y. Hattori and K. Kaneko, *J. Am. Chem. Soc.*, 2003, **125**, 3062; (b) O. Fabelo, L. C. Delgado, J. Pasan, F. S. Delgado, F. Lloret, J. Cano, M. Julve and C. R. Perez, *Inorg. Chem.*, 2009, **48**, 11342; (c) C. Carpanese, S. Ferlay, N. Kyritsakas, M. Henry and M. W. Hosseini, *Chem. Commun.*, 2009, 6786.
- 13 (a) J. C. Jin, Y. Y. Wang, P. Liu, R. T. Liu, C. Ren and Q. Z. Shi, *Cryst. Growth Des.*, 2010, **10**, 2019; (b) J. C. Jin, Y. Y. Wang, W. H. Zhang, A. S. Lermontov, E. K. Lermontova and Q. Z. Shi, *Dalton Trans.*, 2009, 10181; (c) W. H. Zhang, Y. Y. Wang, E. K. Lermontova, G. P. Yang, B. Liu, J. C. Jin, Z. Dong and Q. Z. Shi, *Cryst. Growth Des.*, 2010, **10**, 76.
- 14 (a) H.-L. Jiang and Q. Xu, *CrystEngComm*, 2010, **12**, 3815; (b) L. Han, Y. Zhou, W.-N. Zhao, X. Li and Y.-X. Liang, *Cryst. Growth Des.*, 2009, **9**, 660.
- 15 (a) I. Imaz, D. Maspoch, C. R. Blanco, J. M. P. Falcon, J. Campo and D. R. Molina, *Angew. Chem., Int. Ed.*, 2008, **47**, 1857; (b) J. Yang, J. F. Ma, S. R. Batten and Z. M. Su, *Chem. Commun.*, 2008, 2233; (c) M. Sathiyendiran, J. Y. Wu, M. Velayudham, G. H. Lee, S. M. Peng and K. L. Lu, *Chem. Commun.*, 2009, 3795.
- 16 (a) B. K. Tripuramallu, R. Kishore and S. K. Das, *Inorg. Chim. Acta*, 2011, **368**, 132; (b) P. Lin, W. Clegg, R. W. Harrington and R. A. Henderson, *Dalton Trans.*, 2005, 2388; (c) H. Zhao, Z. R. Qu, H. Y. Ye and R. G. Xiong, *Chem. Soc. Rev.*, 2008, **37**, 84.
- 17 (a) P. K. Dhal and F. H. Arnold, *Macromolecules*, 1992, **25**, 7051; (b) W. Ouellette, H. Liu, C. J. O'Connor and J. Zubieta, *Inorg. Chem.*, 2009, **48**, 4655.
- 18 (a) *CrysAlis CCD and CrysAlis RED, Ver. 1.171.33.55*; Oxford Diffraction Ltd: Yarnton, Oxfordshire, UK, 2008; (b) *SAINTE Software for the CCD Detector System*; Bruker Analytical X-ray Systems, Inc.: Madison, WI, 1998; (c) G. M. Sheldrick, *SADABS: Program for Absorption Correction*; University of Gottingen: Gottingen, Germany, 1997; (d) G. M. Sheldrick, *SHELXS-97: Program for Structure Solution*; University of Gottingen: Gottingen, Germany, 1997; (e) G. M. Sheldrick, *SHELXL-97: Program for Crystal Structure Analysis*; University of Gottingen: Gottingen, Germany, 1997; (f) L. Yang, D. R. Powell and R. P. Houser, *Dalton Trans.*, 2007, 955.
- 19 (a) L. Han, Y. Zhao, W. N. Zhao, X. Li and Y. X. Liang, *Cryst. Growth Des.*, 2009, **9**, 660; (b) P. Pachfule, C. Dey, T. Panda and R. Banarjee, *CrystEngComm*, 2010, **12**, 1600; (c) C. C. Ji, L. Qin, Y. Z. Li, Z. J. Guo and H. G. Zheng, *Cryst. Growth Des.*, 2011, **11**, 480.
- 20 (a) J. Yang, J.-F. Ma, S. R. Batten, S. W. Ng and Y.-Y. Liu, *CrystEngComm*, 2011, **13**, 5296; (b) H.-J. Lee, P.-Y. Cheng, C.-Y. Chen, J.-S. Shen, D. Nandi and H. M. Lee, *CrystEngComm*, 2011, **13**, 4814.

- 21 (a) K. Darling, W. Ouellette, A. Prosvirin, S. Freund, K. R. Dunbar and J. Zubieta, *Cryst. Growth Des.*, 2012, **12**, 2662; (b) Z. Li, M. Li, X.-P. Zhou, T. Wu, D. Li and S. W. Ng, *Cryst. Growth Des.*, 2007, **7**, 1992.
- 22 (a) S. R. Marshall, A. L. Rheingold, L. N. Dawe, W. W. Shum, C. Kitamura and J. S. Miller, *Inorg. Chem.*, 2002, **41**, 3599; (b) M. W. Makinen, L. C. Kuo, M. B. Yim, G. B. Wells, J. M. Fukuyama and J. E. Kim, *J. Am. Chem. Soc.*, 1985, **107**, 5245.